https://doi.org/10.5194/egusphere-2024-3251
Preprint. Discussion started: 13 November 2024

Assessing spatio-temporal variability of firn volume scattering over Greenland with satellite altimeters

Weiran Li [1], Stef Lhermitte [2, 1], Bert Wouters [1], Cornelis Slobbe [1], Max Brils [3, 5], and Xavier Fettweis [4]

[1]Department of Geoscience and Remote Sensing, Delft University of Technology, Delft, the Netherlands
[2]Department of Earth & Environmental Sciences, KU Leuven, Leuven, Belgium
[3]Institute for Marine and Atmospheric Research, Utrecht University, Utrecht, the Netherlands
[4]Spheres research unit, Geography, University of Liège, Liège, Belgium
[5]Geography and Environmental Sciences Department, Northumbria University, Newcastle upon Tyne, UK

Correspondence: Weiran Li (w.li-7@tudelft.nl)

Abstract. In recent decades, satellite radar altimetry has been widely used to assess volume changes over the Greenland Ice Sheet. Especially, melt events result in drastic changes in volume scattering of firn, which induces a pronounced change in parameters derived from radar altimetry. Due to the recent and increasingly frequent melt events over Greenland, the impacts of these events on the firn condition i.e. formation of ice lenses and reduction of firn air content, need to be better understood. This study therefore exploits the ability of long-term CryoSat-2 data in indicating changes in firn volume scattering, in order to assess the spatio-temporal firn condition variations in Greenland. More specifically, this study utilises the leading edge width (LeW) parameter derived from CryoSat-2 Low Resolution Mode, which has been proven to be the parameter most sensitive to changes in volume scattering, and assesses its variation between January 2011 and August 2021. With a combined analysis of remote sensing observations, in situ observations and outputs from regional climate models, our study demonstrates that the LeW drop induced by extreme melt events in the interior of Greenland experiences a gradual recovery, which can potentially be explained by new snow deposition. However, in many high-elevation regions of Greenland where firn layers were originally dry, due to the recently recurring extensive melt, the firn volume scattering does not fully recover to the original state before the 2012 melt, indicating a long-lived increase in Greenland's firn density in a changing climate. Finally, our study also confirms the capability of using radar altimeter data to monitor changes in volume scattering properties of firn in the long-term.

1 Introduction

Over the recent decades, the Greenland Ice Sheet has experienced a notable increase in the frequency and intensity of melt events (Tedesco et al., 2011, 2013; Nilsson et al., 2015; Tedesco et al., 2016; Tedesco and Fettweis, 2020). These events are particularly prevalent in low-elevation regions, where they contribute to runoff towards the ocean. This runoff negatively impacts the surface mass balance (SMB) of the ice sheet and may lead to irreversible ice loss and sea-level rise (Lenton et al., 2008; Sasgen et al., 2012). In contrast, at higher elevations, meltwater can infiltrate and refreeze within the porous firn (Harper et al., 2012). This refreezing process releases latent heat, which accelerates firn compaction and diminishes the firn's capacity to store additional meltwater, consequently speeding up runoff from the ice sheet's interior (van den Broeke et al.,

https://doi.org/10.5194/egusphere-2024-3251
Preprint. Discussion started: 13 November 2024

2016; Machguth et al., 2016; Vandecrux et al., 2019). Surface meltwater also drains towards the bedrock through crevasses and moulins, altering basal frictions and ice velocities (Zwally et al., 2002; Sundal et al., 2011; Meierbachtol et al., 2013). Furthermore, studies suggest that the runoff and melt will continue to increase (Vizcaíno et al., 2009; Huybrechts et al., 2011). Therefore, the determination of melt and refreezing in the firn layer over Greenland has become of utmost importance for understanding the ice sheet's overall stability and response to climate change (Heilig et al., 2018).

Remote sensing techniques are essential for long-term, spatio-temporally continuous monitoring of melt and refreezing events over the Greenland ice sheet, as in situ data are sparse in both space and time (Hall et al., 2008; Koenig et al., 2016; Castelao and Medeiros, 2022). Radar and lidar altimetry sensors, primarily used to measure surface height (changes) (Helm et al., 2014b; Slater et al., 2018), can provide information on melt and refreezing events with much greater coverage. They do this indirectly, as refreezing impacts firn density, firn air content (FAC) and grain size (Vandecrux et al., 2019; Brils et al., 2022), which further influence the altimetry signals through changes in volume and surface scattering (Fahnestock et al., 1993; Adodo et al., 2018; Alley et al., 2018; Larue et al., 2021).

Various studies have focused on deriving firn properties from the waveform of the returned radar signal in radar altimetry. For example, the European Space Agency (ESA) CryoSat-2 satellite, equipped with a radar altimeter operating at Ku-band (13.575 GHz) frequency, has been employed to track the formation of ice lenses following melt events (Nilsson et al., 2015), to understand the impact of volume scattering properties on height estimations (Simonsen and Sørensen, 2017), and to derive surface snow properties such as roughness and density (Scanlan et al., 2023). Nilsson et al. (2015) and Simonsen and Sørensen (2017) showed that leading edge width (LeW) is an indicator of volume scattering, while Nilsson et al. (2015) in particular observed the impact of the 2012 Greenland melt event and its subsequent refreezing on the parameters derived from radar waveforms, including LeW, trailing edge slope (TeS) and peakiness, backscatter intensity and height. The Simonsen and Sørensen (2017) study indicated that within the Low Resolution Mode (LRM) coverage, LeW could be effectively used to correct for height biases caused by volume scattering. Furthermore, Scanlan et al. (2023) developed a model using CryoSat-2 waveforms to derive surface roughness and density of snow in Greenland between 2013 and 2019. Finally, using data from NASA's Operation IceBridge (OIB) mission, i.e. data from the Multichannel Coherent Radar Depth Sounder (MCoRDS) and Airborne Topographic Mapper (ATM) laser altimeter, Rutishauser et al. (2024) assessed the relation between vertical offsets in the radar surface reflection and the vertical heterogeneity caused by melt events. In addition, although the study was conducted over Antarctica, Michel et al. (2014) analysed the height differences between radar (ENVISAT) and laser (ICESat) altimeters to derive Ku-band radar penetration depths into firn and compared these height differences with LeW, providing insights into opportunities for similar approaches to study Greenland's firn.

Despite the advances in using altimetry to monitor Greenland's firn, the evaluation of firn properties has been limited to either to periods without extensive melt (e.g. January 2013 to January 2019; Scanlan et al., 2023) or small regions (e.g., NEEM site; Nilsson et al., 2015). However, the availability of over a decade of CryoSat-2 data, offers an opportunity for long-term studies of Greenland's firn scattering properties. Following previous studies, we focus on two self-derived parameters: the LeW and the height difference between ICESat-2 and CryoSat-2, which both will be used to provide insights into the volume scattering of Greenland firn. The LeW is adopted as it is sensitive to volume scattering variations (Legrésy and Rémy, 1997; Nilsson

https://doi.org/10.5194/egusphere-2024-3251
Preprint. Discussion started: 13 November 2024

et al., 2015). The height difference between ICESat-2 and CryoSat-2 is used as an indicator of penetration depths, as Ku-band radar has a larger penetration depth than ICESat-2 green light (Michel et al., 2014; Smith et al., 2018).

Furthermore, recent developments in climate and firn models, such as the Modèle Atmosphérique Régionale (MAR) (Fettweis et al., 2011, 2017; Lambin et al., 2022) and the Firn Densification Model from the Institute for Marine and Atmospheric research Utrecht (IMAU-FDM v1.2G; Brils et al., 2022), provide spatially and temporally continuous firn property data. By comparing long-term LeW measurements with firn properties from climate and firn models, we analyse how spatial and temporal variations in firn properties affect LeW and to improve the interpretation of radar altimeter scattering properties for future research. Additionally, we expect the height difference between laser and radar altimeters to offer further insights into firn volume scattering, complementing the interpretation of LeW time series (Michel et al., 2014). Finally, to understand the LeW variations, we have to understand both volume scattering and surface scattering, which can influence the LeW variations to different extents (Michel et al., 2014; Nilsson et al., 2015). Therefore, we also interpret the LeW variations derived from our study with the help of the results from previous studies, i.e. Scanlan et al. (2023) and Rutishauser et al. (2024).

The objective of this paper is, therefore, to assess long-term changes over the Greenland Ice Sheet. For this purpose, we present the spatio-temporal variations of LeW between 2011 and 2021 and of the difference between ICESat-2 and CryoSat-2 height estimations between 2019 and 2021 over the interior of Greenland, and to subsequently assess whether such variations can reflect the variations in firn properties by comparing them with variations in modelled firn density and FAC provided by MAR and IMAU-FDM. The details of data and coverage are described in Section 2. The derivation of LeWs and height differences between ICESat-2 and CryoSat-2 will be detailed in Section 3. Sections 4 and 5 present, analyse and discuss the results. Finally, our main findings and outlook are presented in Section 6.

2 Data

This section introduces the datasets used to assess how the CryoSat-2 time series can indicate the impact of recurrent melt–refreezing on Greenland's firn, with a focus on time series of LeW derived from CryoSat-2, and height difference between ICESat-2 and CryoSat-2. The time series of satellite data are complemented by reference datasets for a comprehensive interpretation of volume and surface scattering variations.

2.1 CryoSat-2 observations

CryoSat-2 LRM data acquired over the interior of the Greenland ice sheet provide waveform information which can be further processed to obtain various parameters (Nilsson et al., 2015; European Space Agency, 2019; Meloni et al., 2020). The acquisition period of the CryoSat-2 LRM Baseline D data we use in this study is between January 1, 2011 and August 31, 2021. The LeW in metres is computed from the normalised waveform as

$$LeW = (b_{0.99} - b_{0.01})S_r \quad (1)$$

https://doi.org/10.5194/egusphere-2024-3251
Preprint. Discussion started: 13 November 2024

where $b_{0.99}$ and $b_{0.01}$ are the range bias corresponding to the bins where the normalised waveform power equals 0.99 and 0.01, respectively (found with linear interpolation), and S_r is the range resolution of CryoSat-2 LRM.

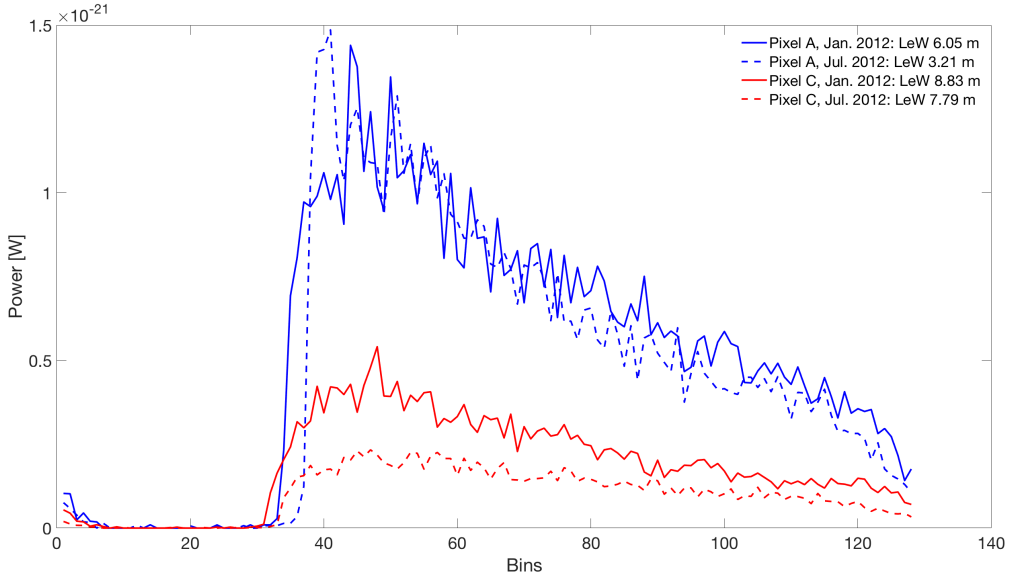

Figure 1. Waveform examples from different regions of interest in different periods. Pixel A and pixel C refer to the highlighted pixels in Fig. 3.

Subsequently, we derive height estimations of CryoSat-2 (h_C) from the waveforms using the Offset Centre of Gravity (OCOG) retracker (Wingham et al., 1986; Bamber, 1994; Gommenginger et al., 2010) with a 50% threshold. Such a high 50% threshold corresponds to the radar return within the firn and is expected to indicate the volume scattering of Ku-band radar in the firn layer (Li et al., 2022). To correct for slope-induced errors in the h_C height estimation, we use the leading edge point-based (LEPTA) method from Li et al. (2022), as it utilises a high-resolution digital elevation model (DEM) and has the advantage to account for impacts of complex terrains.

To demonstrate the typical waveforms under different conditions and the corresponding LeWs, we provide examples of waveforms before (January) and after (July) the extensive 2012 melt event (Tedesco et al., 2013) in different regions of interest in Fig. 1: pixel A corresponds to the vicinity of the NEEM site as studied by Nilsson et al. (2015), where the difference between January and July 2012 shows reduced volume scattering due to the 2012 melt event. Pixel C corresponds to the region with constantly high surface roughness as derived by Scanlan et al. (2023), where a rougher surface typically corresponds to a higher LeW and less pronounced differences before and after the melt, potentially due to the dominant role of surface scattering from a constantly rough surface.

Finally, the derived LeWs are grouped into grids with two different resolutions. A 50 km×50 km grid is used to observe the variations along a north-south transect, as this resolution both ensures a sufficient division over the interior of Greenland

https://doi.org/10.5194/egusphere-2024-3251
Preprint. Discussion started: 13 November 2024

and a sufficient amount of data per month per pixel. A 25 km×25 km grid is adopted when the data from multiple months are aggregated for the analysis. The mean LeW of all points within each pixel is calculated and utilised.

2.2 ICESat-2 observations

To assess the volume scattering variation of CryoSat-2, we derive the height variation of CryoSat-2 with respect to a reference surface height as a measure for volume scattering properties; the ICESat-2 L3A Land Ice Height (ATL06) product Version 5 (Smith et al., 2020) is hence used as the reference surface. ICESat-2 uses the Advanced Topographic Laser Altimeter System (ATLAS) with laser at a 532 nm wavelength (Abdalati et al., 2010). The along-track resolution of ATL06 product is ~ 40 m (Smith et al., 2023), and the geolocation bias is less than 10 m (National Snow and Ice Data Center (NSIDC), 2021). In this study, we use ATL06 between January 1, 2019 and August 31, 2021 to obtain ICESat-2 heights (h_{ICE2}) for each CryoSat-2 point (h_C). The ATL06 data do not have a fixed or regularly gridded resolution, therefore we use a natural-neighbour interpolation to obtain ICESat-2 heights (h_{ICE2}) at each CryoSat-2 point (h_C). For each CryoSat-2 point, the ICESat-2 points within 50 m and acquired within the same month are selected for this interpolation. Over a sloping terrain, extra height differences between h_C and h_{ICE2} can be caused by potential topography differences within the 50 m distance. To correct for this topography-induced difference, we bi-linearly interpolate (due to the regular resolution) the reference DEM (100 m ArcticDEM) to both the CryoSat-2 (h_{DEMC}) and ICESat-2 (h_{DEMI}) locations; hence, the differences between the ICESat-2 and CryoSat-2 heights (Δh) is calculated as

$$\Delta h = h_{\text{ICE2}} - h_C - (h_{\text{DEMI}} - h_{\text{DEMC}}) \tag{2}$$

The spatial distribution as well as the overall probability distribution of Δh between January 2019 and August 2021 are visualised in Fig. 2. However, when the radar altimeter waveform is dominated by surface scattering, a 50 % threshold retracker can still result in an underestimated or negative penetration depth (Davis, 1997). In addition, for the analysis where we compare and interpret the spatio-temporal variations with firn properties, we need to select a valid penetration depth that corresponds to the vertical resolution of the available firn models (i.e., MAR and IMAU-FDM) to ensure a fair comparison. Figure 2 shows that Δh is generally between 0 and 1.5 m on the interior of the ice sheet, therefore this range is used to select valid Δh that can be used as an indicator of volume scattering.

2.3 Reference DEM

The ArcticDEM is used to (i) correct the CryoSat-2 LRM height estimations for slope-induced errors with the LEPTA correction method (Li et al., 2022), and (ii) divide the Greenland ice sheet into different elevation groups for the spatio-temporal analysis. The ArcticDEM is constructed from recent stereo satellite imagery (Porter et al., 2023) with a systematic error below 5 m (Noh and Howat, 2015). The ArcticDEM is available in different resolution, ranging from 2 m to 1 km (Porter et al., 2023). For computational efficiency, we first use the 100 m resolution ArcticDEM to correct for slope-induced errors in deriving CryoSat-2 height estimations (Li et al., 2022). To assess the impact of the topography on the spatial variability of LeWs, we use the 1 km resolution ArcticDEM in the subsequent spatio-temporal analysis due to computational efficiency.

https://doi.org/10.5194/egusphere-2024-3251
Preprint. Discussion started: 13 November 2024

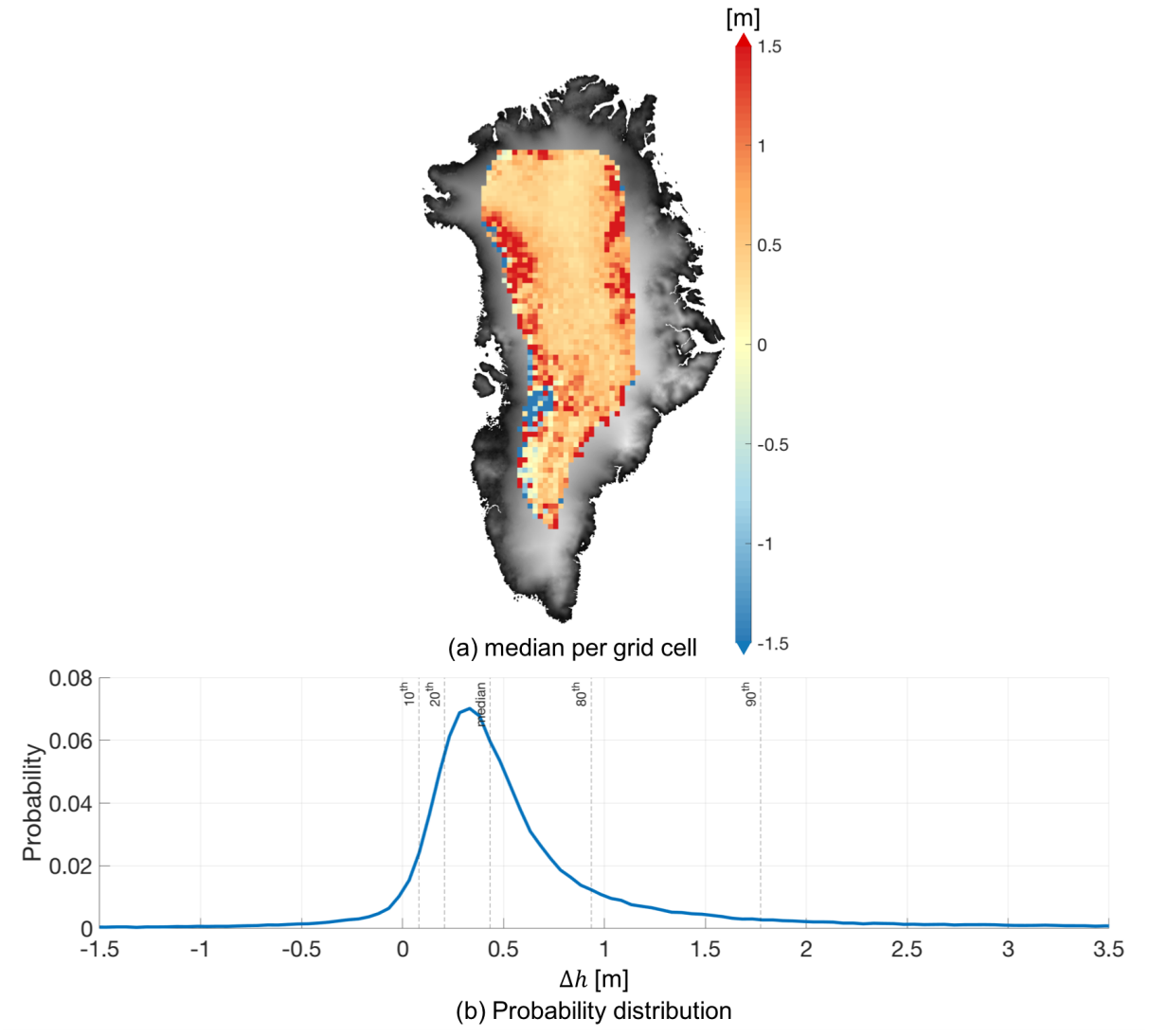

Figure 2. Statistics of height difference between ICESat-2 and CryoSat-2 (Δh). (a) is the median Δh per grid cell in a 25 km $\times$25 km grid; the background is the 1 km $\times$1 km DEM from Helm et al. (2014a, b). (b) is the probability distribution function of Δh with percentiles labelled in vertical lines.

https://doi.org/10.5194/egusphere-2024-3251
Preprint. Discussion started: 13 November 2024

2.4 Firn models

To support the interpretation of the altimeter-derived parameters (LeW and Δh), we use firn density, melt water content (MWC) and firn air content (FAC) from two different regional climate and firn models, the Modèle Atmosphérique Régional (MAR, Section 2.4.1) and IMAU Firn Densification Model (IMAU-FDM, Section 2.4.2) respectively.

2.4.1 Modèle Atmosphérique Régional (MAR)

Layered firn densities and melt water content (MWC) over the study period are obtained from the version 3.12 Modèle Atmosphérique Régional (MAR) forced by the ERA5 reanalysis (Fettweis et al., 2017; Lambin et al., 2022). The MAR outputs have a spatial (horizontal) resolution of 10 km and a daily temporal resolution, whereas the vertical resolution of the snowpack varies in time between 1 cm close to the surface to 5 m at the bottom of the snowpack. The MAR model resolves here the 20 first metres of snow only and the weighted average density of the upper 1.5 m (a threshold based on Fig. 2) is calculated based on the depth of each snow layer thickness. The firn density profile can be used to infer the amount of volume scattering. For example, the presence of a refrozen layer (i.e. a layer with high density; Nilsson et al., 2015; Otosaka et al., 2020) prevents the penetration of the radar signal, hence reduces the volume scattering.

The MWC is used to restrict our analysis to non-melt conditions, in order to reduce the impact of meltwater production on Ku-band radar and 532 nm laser. When MWC> 0, meltwater is present in the firn layer, hence the altimeter-derived parameters as well as the densities should be excluded. A nearest-neighbour interpolation is performed to identify the MWC values at each CryoSat-2 location.

To assess the timing and extent of melt–refreeze patterns, the meltwater production and refreezing outputs of MAR (in the unit of mmWE day^{-1}) are used as reference. To provide insights into volume scattering variations, the total snow height change (i.e. the snowfall accumulation) from MAR is adopted. We calculate the accumulated total snow height change as the sum of daily total snow height change from date of the intensive melt (July 12, 2012; Nghiem et al., 2012) to August 31, 2021. The time series of these outputs are visualised in Appendix A.

2.4.2 Firn Densification Model (IMAU-FDM)

Alternatively, firn density, MWC and FAC with a 10-day temporal resolution are obtained from the firn density model IMAU-FDM v1.2G (Brils et al., 2022). It is a Lagrangian 1D firn model which computes the evolution of the firn thickness, density, temperature and water balance. It uses a "bucket method" for computing meltwater percolation into the firn. Its ability to accurately model firn properties has been validated in Brils et al. (2022). At its surface, IMAU-FDM is forced by the output of the polar version of the Regional Atmospheric Climate Model (RACMO2; Noël et al., 2018). Results from the model are available between October 1957 and December 2020. Similarly to the MAR data, we (i) masked out all FDM data when the MWC is positive and (ii) averaged the density over the top 1.5 m.

The FAC is the vertically integrated porosity in the firn (Kuipers Munneke et al., 2015), which is in the unit of metres. While the density is calculated over the first 1.5 m but the FAC is calculated for the entire firn column. FAC is the total porosity of firn,

https://doi.org/10.5194/egusphere-2024-3251
Preprint. Discussion started: 13 November 2024

indicating the capability of the firn layer to retain meltwater (Vandecrux et al., 2019). Therefore, we use the modelled FAC time series to validate whether the melt–refreeze pattern we aim to observe has a large impact on firn conditions. The application of this dataset is two-fold. First, to support the interpretation of LeW time series, we use IMAU-FDM firn density and FAC as a reference dataset to compare with both LeW and MAR density monthly time series between January 2011 and December 2020. Second, to learn about the most recent changes of Greenland ice sheet with respect to previous decades, we derive a long-term time series (between 1961 and 2020) by computing the yearly average of the IMAU-FDM density and FAC. In addition, while FAC increases with elevation and can have a large spatial variation, i.e. approximately 0 towards the margins and more than 20 m in the interior of the ice sheet, the juxtaposed FAC over the entire studied area shows pronounced spatial variation and little temporal variation. Therefore, the temporal variation needs to be enhanced with respect to the spatial variation in FAC. For this purpose, we remove the long-term mean of each pixel (using the same grids as the resampled CryoSat-2 LeW) from the time series.

2.5 In situ density acquisitions

Besides the firn model data, we also use available in situ density profiles from Schaller et al. (2016b); Otosaka (2020) at different locations to show the impact of melt events on firn layers. In situ measurements are helpful in providing insights into whether and where refrozen layers persist within the Greenland firn, which support the interpretation of the LeW variations. We use available and published in situ densities in our analysis if: (i) the acquisition site is within the CryoSat-2 LRM coverage; (ii) the acquisition contains the 2012 melt layer to provide information on the existence and depth of refrozen ice layers, (iii) the acquisition is vertically continuous, instead of one measurement at a single depth. Therefore, on the one hand, we rely on the 2 m depth firn core densities from Schaller et al. (2016b) along a trajectory between NEEM and East Greenland Ice-core Project (EGRIP), which were obtained using X-ray tomography in May 2015 (Schaller et al., 2016a). Due to the dense spatial (horizontal) sampling of the Schaller et al. (2016b) density measurements (22 measurements in total), we select the measurements at NEEM, N2E06 and EGRIP (Schaller et al., 2016a) as representative reference data. On the other hand, we use firn core densities from Otosaka (2020) along the Expédition Glaciologique Internationale Au Groenland (EGIG) line, specifically at T12, T19, T30 and T41, which were obtained using stratigraphy in May 2017 (Otosaka et al., 2020). The locations and corresponding densities are shown in Fig. 3.

2.6 Stratigraphy, roughness and topography

In addition to the modelled firn properties and in situ densities, we use the vertical stratigraphy derived from Rutishauser et al. (2024) to understand the formation of melt-induced ice layers. Furthermore, we can analyse the performance and sensitivity of the derived LeW to the melt events by comparing the LeW with the stratigraphy dataset. The stratigraphy is represented by the vertical offsets between the ice surface height obtained by the OIB ATM laser altimeter, and the 195 MHz OIB MCoRDS, acquired simultaneously between 2011 and 2019, computed as

$$dz = h_{laser} - h_{radar} \tag{3}$$

https://doi.org/10.5194/egusphere-2024-3251
Preprint. Discussion started: 13 November 2024

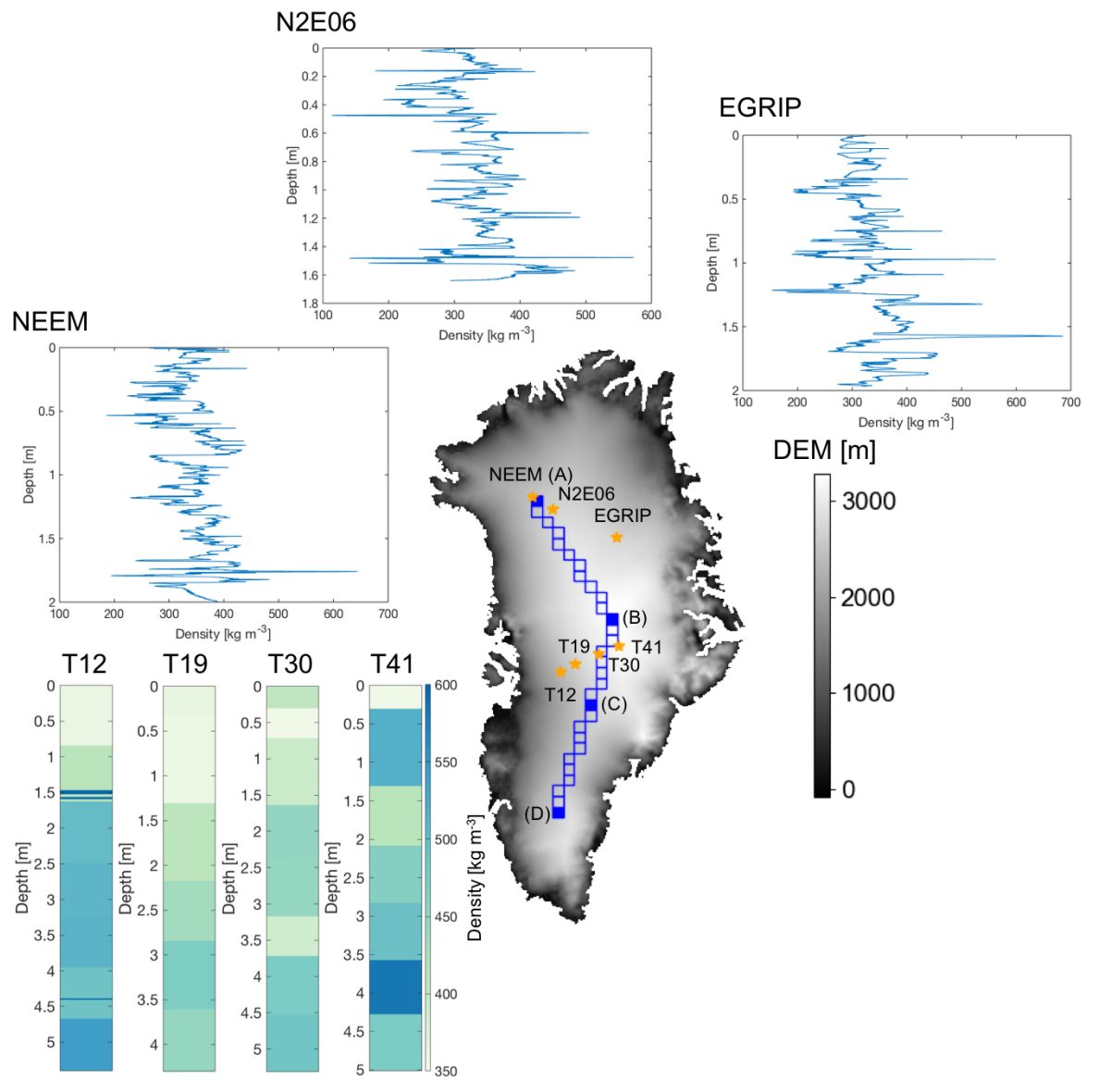

Figure 3. In situ densities and locations of measurements: the NEEM, N2E06 and EGRIP measurements are from Schaller et al. (2016b), and the T12, T19, T30 and T41 measurements are from Otosaka (2020). The background is the 1 km $\times$1 km DEM from Helm et al. (2014a, b). Blue rectangles represent the transect of interest used in Section 3. Several regions of interest are highlighted with filled blue rectangles, and are taken as examples for a separate time series analysis.

https://doi.org/10.5194/egusphere-2024-3251
Preprint. Discussion started: 13 November 2024

where h_{radar} is the height derived by picking the optimal peaks in MCoRDS surface returns, and h_{laser} is the mean height of all laser observations within MCoRDS' pulse-limited footprint. The obtained dz values correspond with firn stratigraphy (a low dz corresponds to a homogeneous vertical structure). Since dz increases with the vertical heterogeneity of the firn, an increase in dz indicates the formation of refrozen layers (Rutishauser et al., 2024). The dz dataset contains 15.5 million data points with an annual temporal resolution (Rutishauser et al., 2024).

Additionally, we use the surface roughness dataset derived by Scanlan et al. (2023) to analyse under which circumstances the LeW variation is dominated by surface scattering, since LeW can also be affected by topography and surface roughness (Legrésy and Rémy, 1997; Li et al., 2022). The dataset was created by adopting the Radar Statistical Reconnaissance (RSR) technique in combination with a backscattering model. The temporal coverage of the dataset is between 2013 and 2019 with a monthly resolution.

As an indicator of topography, the standard deviation of the 1 km ArcticDEM elevations per 50 km$\times 50$ km pixel along the north–south transect as well as the standard deviation of ArcticDEM elevations grouped by the aforementioned 10 DEM groups are computed. The ArcticDEM is temporally invariant, therefore only the spatial variation of the standard deviations are presented and analysed.

3 Method

Since LeW variations are driven by both surface and volume scattering, especially melt and subsequent refreezing, we present a qualitative study of the relationship between LeW variations and melt–refreezing events.

3.1 Assessment of LeW's ability to indicate scattering variations

Since LeW variations can be affected by variations in both volume and surface scattering, we first perform a comparison with the available remote sensing data of stratigraphy and roughness (see Section 2.6).

First, to assess the potential of LeW in indicating the spatio-temporal variability in volume scattering, we compare LeWs with dz values derived by Rutishauser et al. (2024). Due to the large amount of dz points, we compute the mean dz values per OIB campaign over the 25 km $\times 25$ km grid consistent to the resampled resolution of LeW. Finally, we mask out grid cells where either dz values or LeWs are not available.

Second, we compare the LeW data with the available roughness and topography data as spatio-temporal LeW variations can also be affected by surface scattering, which is composed of surface scattering and topography (Michel et al., 2014; Li et al., 2022). Therefore, on the one hand, we use the Scanlan et al. (2023) roughness data to represent the wavelength-scale surface roughness. We first resample the Scanlan et al. (2023) data to the 50 km$\times 50$ km grid same as the LeW. The time series analysis of LeW and roughness data is two-fold, where we juxtapose LeW and roughness data both (i) along a geographical transect connecting the NEEM site (Nilsson et al., 2015; Schaller et al., 2016a), Summit Camp and South Greenland and (ii) along 10 different averaged elevation bands between 100 m and 3280 m. On the other hand, we also compare the LeW data with the ArcticDEM standard deviation in order to assess the impact of macro-scale roughness due to topographic variation on LeW.

https://doi.org/10.5194/egusphere-2024-3251
Preprint. Discussion started: 13 November 2024

3.2 Correlation analysis between LeW and Δh

Since Δh is a typical indicator of radar altimeter penetration depth (Michel et al., 2014), we compute the correlation between all LeW and Δh estimates to assess to what extent the LeW variation is dominated by the penetration depth hence volume scattering. For this purpose, we adopt the 25 km$\times$25 km grid introduced in Section 2.1. Within each grid cell, the Pearson correlation coefficients are computed between LeW and Δh for all valid Δh estimations throughout the entire studied period. Furthermore, to assess the reliability of the derived correlation between parameters, a p-value representing the significance of the correlation is computed for each correlation coefficient; the correlation coefficient is insignificant when the p-value exceeds 0.05 (Bermudez-Edo et al., 2018).

3.3 Interpretation of LeW's spatio-temporal variation

Following the previous analysis, we adopt the 50 km$\times$50 km grid over Greenland to obtain sufficient monthly LeW data (as mentioned in Section 2.1) between 2011 and 2021. After the monthly gridded LeWs are obtained, we compute the average LeW between January and May every year, and assess the difference in the averaged LeW between (i) every year and its previous year, and (ii) every year and 2011, respectively. With the first comparison, we asses the annual changes in volume scattering as melt events typically occur within summer season (June to August) (Tedesco and Fettweis, 2020). With the second comparison, we assess the LeW recovery since the extreme 2012 melt event (Tedesco et al., 2013).

To analyse the LeW variation with respect to the modelled firn properties, we perform the same two-fold time series analysis as proposed in Section 3.1, where the spatio-temporal variations of LeW, FAC, MAR densities and IMAU-FDM densities are juxtaposed and compared. The comparison is performed over two different time periods. The first one is between 2011 and 2021, when the CryoSat-2 Baseline D data are available. This comparison is purely to assess the capability of LeW to indicate firn processes. The second comparison is performed between 1960 and 2020, when IMAU-FDM data are available. This comparison is a supportive assessment to understand whether the firn processes are recent, and to provide insight and indications for future studies.

4 Results

4.1 LeW time series compared with vertical stratigraphy

Figure 4 presents the time series of vertical stratigraphy dz, alongside the time series of LeW. Both dz and LeW are generally high near the western margins, reaching up to around 2 m and 25 m, respectively. In contrast, both values are low in the high-elevation interior of the ice sheet, with dz ranging from -0.2m to 0.1m and LeW between 5 m and 8 m. However, in the southwest ablation zone, a low dz of around 0.1 m is observed, while LeW remains high at approximately 25 m.

dz is approximately 0.5 m higher in 2013 than in the earlier years, but decreases to lower values between 2014 and 2019. In contrast, the reduction in LeW persists over a longer period. During the period from 2013 to 2019, LeW values from CryoSat-2 are 2 m to 3 m lower compared to the period between 2011 and 2012.

https://doi.org/10.5194/egusphere-2024-3251
Preprint. Discussion started: 13 November 2024

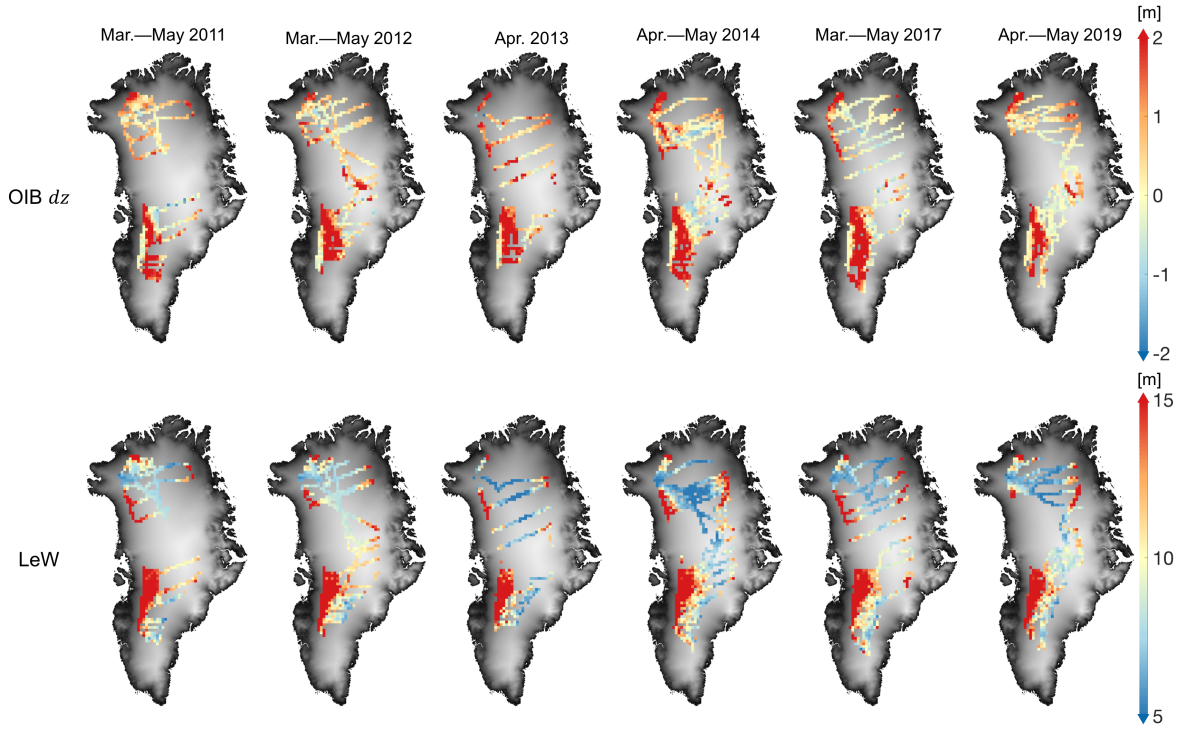

Figure 4. Upper: dz computed by Rutishauser et al. (2024); lower: LeW in the corresponding time of acquisition as dz. The background is the 1 km $\times$1 km DEM from Helm et al. (2014a, b) focusing on Greenland.

Increases in dz are linked to the formation of ice slabs (Rutishauser et al., 2024). The recovery of dz after 2013 suggests that the deposition of new snow between 2014 and 2019 covered the ice slabs beyond the MCoRDS' penetration depth. However, our LeW time series indicates that this recovery is not reflected in the volume scattering, as LeW continues to show reduced scattering due to subsurface high-density layers. This reduced volume scattering is consistent with the elevated firn densities shown in Figure 3. At locations such as N2E06, EGRIP and T12, thin (approximately 0.1 m) high-density (more than 500 $kg\ m^{-3}$) layers persist at around 1.5 m in 2015 or 2017.

4.2 Assessment of the contribution of surface scattering to LeW variations

The comparison of the LeW and surface roughness time series between 2013 and 2019, shown in Figures 5a and c, reveals a clear correspondence between these two variables. Zones of high surface roughness (greater than 6×10^{-4} m) coincide with elevated LeW values (greater than 9 m) around pixels C and D. The region south of pixel C corresponds to Fig. 4 of van den Broeke et al. (2023), where the modelled melt extent exceeds 10 $kg\ m^{-2}\ yr^{-1}$. Similarly, in Figures 5b and d, regions with high LeW (greater than 14 m) are associated with increased surface roughness (greater than 8×10^{-4} m) at elevations below 1800 m.

https://doi.org/10.5194/egusphere-2024-3251
Preprint. Discussion started: 13 November 2024

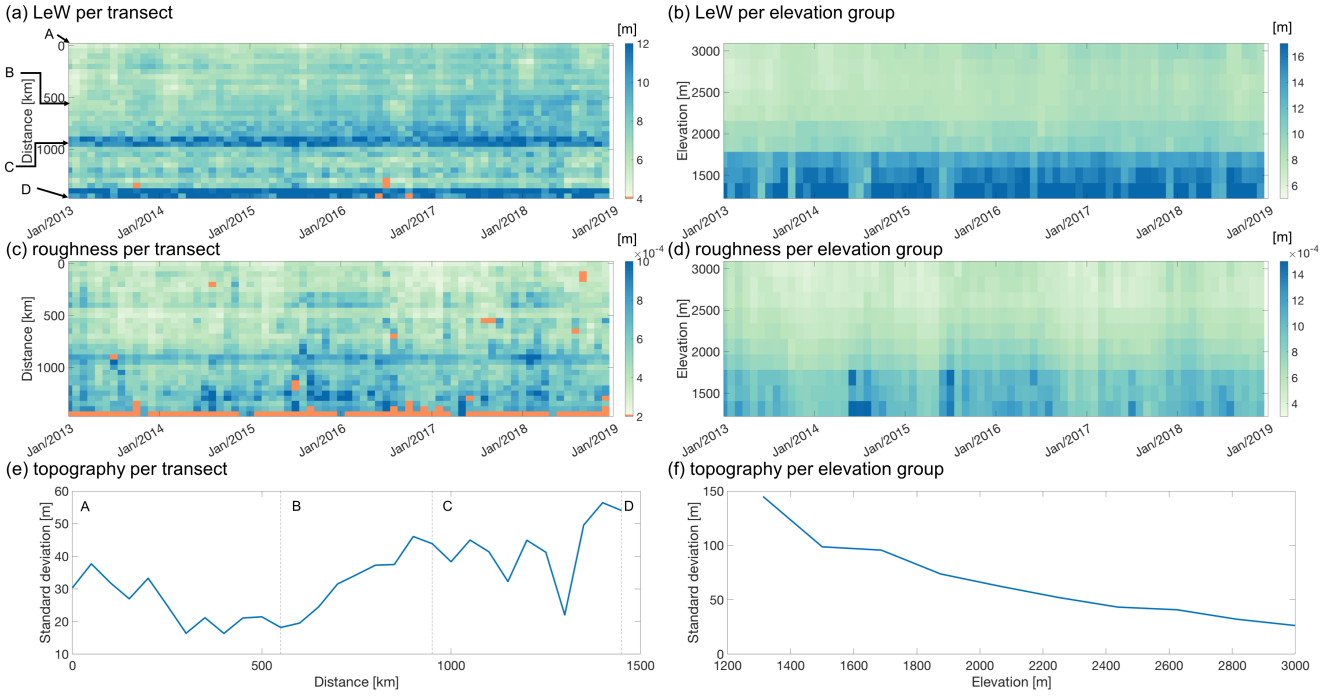

Figure 5. (a),(c),(e) LeW, surface roughness (represented by surface root mean square (RMS) height in unit of metres) and variability of the topography (represented by the standard deviation of ArcticDEM per 50 km pixel) along the north–south transect, respectively. A–D correspond to the inspected pixels highlighted in Fig. 3. (b),(d),(f) LeW, surface roughness and topography grouped by the 10 elevation bands, respectively. Orange colour indicates that the data are not available.

Figure 5e demonstrates that the spatial variation in topography follows a similar pattern to the LeW (Fig. 5a), with a high standard deviation of elevation per grid cell (greater than 50 m) around pixel D, where the roughness data is not available. Figure 5f shows that the complexity of the topography decreases with increasing elevation, a trend that mirrors the LeW pattern in Figure 5b, where LeW generally increases as elevation decreases.

This combined analysis of surface roughness and topography indicates that LeW tends to increase in areas where surface roughness is high and the topography is complex.

4.3 Assessment of correlation between LeW and Δh

Figure 6 presents the correlation coefficients between the Δh and LeW time series for each 25 km×25 km grid cell. Overall, within the CryoSat-2 LRM coverage, LeW and Δh exhibit a generally positive correlation, with a median value of approximately 0.3. The histogram in Figure 6c further highlights that the correlation between LeW and Δh tends to be positive over the study areas.

https://doi.org/10.5194/egusphere-2024-3251
Preprint. Discussion started: 13 November 2024

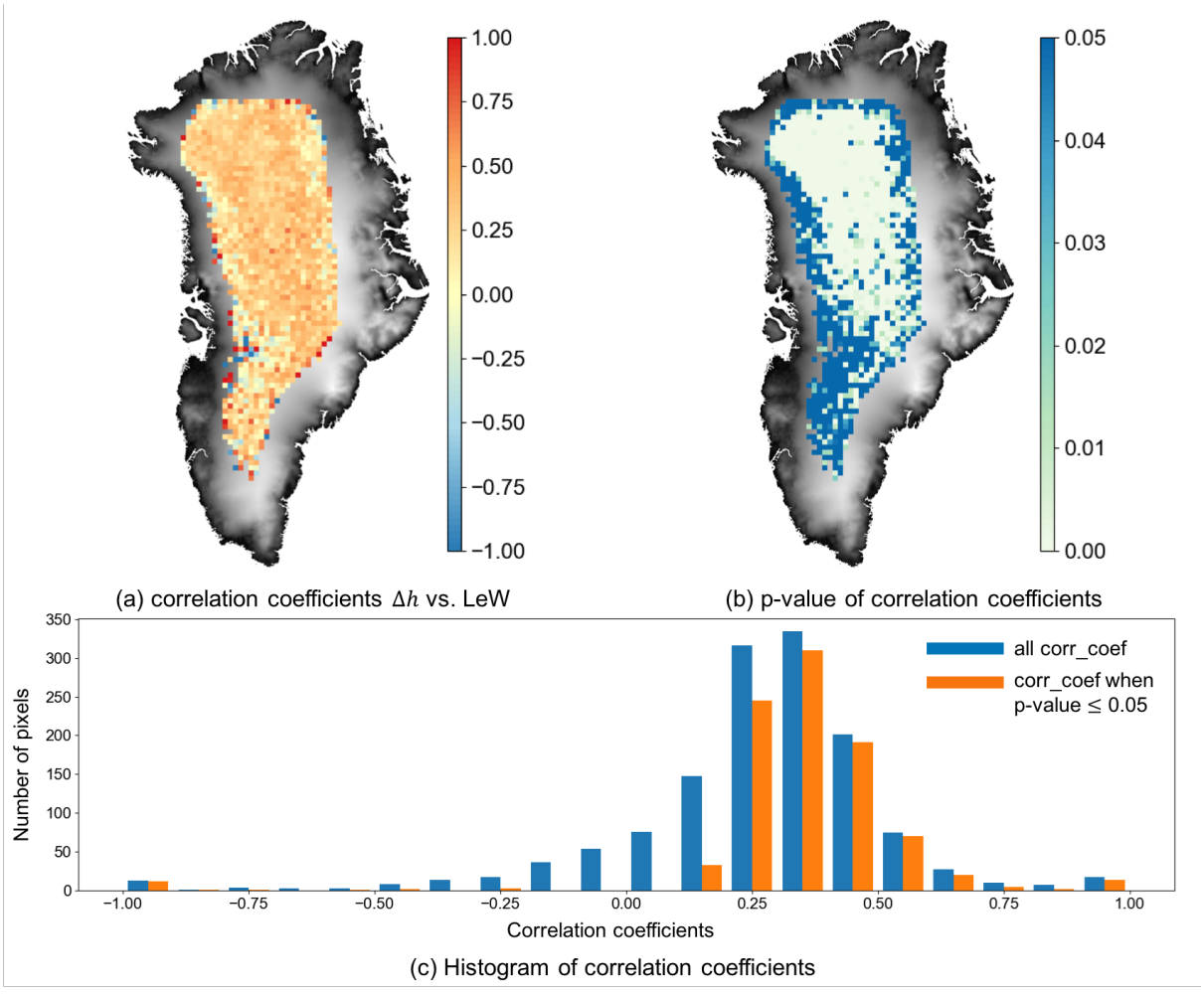

Figure 6. (a) Map of correlation coefficients between Δh and LeW, and (b) map of p-values of correlation coefficients between Δh and LeW. The background is the 1 km $\times$1 km DEM from Helm et al. (2014a, b) focusing on Greenland. (c) Histogram of correlation coefficients when all correlation coefficients are considered in blue, and when only significant correlation coefficients are considered (p-value≤ 0.05) in orange.

https://doi.org/10.5194/egusphere-2024-3251
Preprint. Discussion started: 13 November 2024

The significance of these correlations, as indicated by the p-values, shows that the correlation coefficients are generally more significant in the interior of the ice sheet compared to the margins. When applying a threshold (0.05) on the p-value to focus on pixels with high significance, the median correlation coefficient increases to 0.4. The lower correlation and significance towards the margins can likely be attributed to higher surface scattering, which is caused by surface roughness and topographic variation (Legrésy and Rémy, 1997; Nilsson et al., 2015), as demonstrated earlier in Section 4.2.

The positive correlation between LeW and Δh suggests that as LeW increases, the penetration depth of CryoSat-2 also increases, indicating a rise in volume scattering. However, the correlation coefficients remain below 0.5 overall. This aligns with the findings of Nilsson et al. (2015), which showed that LeW was more sensitive to ice-lens formation and volume scattering variations than Δh. Nevertheless, LeW was used as an indirect parameter to assess volume scattering, particularly when ICESat-2 data were not available.

4.4 Assessment of inter-annual LeW variations

Figure 7a presents the differences in averaged winter–spring LeW between consecutive years. It shows a significant reduction (greater than 2 m) in LeW over the interior of the ice sheet between 2012 and 2013, followed by a recovery between 2013 and 2015, with an increase of approximately 0.5 m. This initial reduction in 2012—2013 indicates a decrease in volume scattering, corresponding to the extreme melt event and subsequent ice-lens formation in 2012 (Tedesco et al., 2013; Nilsson et al., 2015). The recovery between 2013 and 2015 suggests a return to stronger volume scattering, likely due to new snow deposition hence the downward movement of ice lenses (Rennermalm et al., 2021).

Similarly, between 2018 and 2019, LeW experiences another minor drop of about 1 m, which coincides with the early melt observed in April and May 2019 (Tedesco and Fettweis, 2020) and the strong melt events between June and December 2018 that reduced volume scattering. Between 2019 and 2020, LeW increases are observed in the northern part of the ice sheet, while decreases are noted in the southeast.

Figure 7b compares the average LeW (from January to May) of each year with the average LeW of 2011, highlighting long-term variations relative to the extreme melt year of 2012. All years show a negative difference in the interior of the ice sheet, except for the difference between 2011 and 2012, indicating that after the 2012 melt, LeW does not fully recover. It remains approximately 2 m below 2011 levels in the centre of the ice sheet. The area with negative values (i.e., no LeW recovery since 2012) shrinks between 2013 and 2018, expands again in 2019, and remains stable between 2019 and 2021.

When combining Figs. 7a and b, a notable recovery in LeW since 2012 is evident. This recovery can be attributed to new snow deposition on top of the ice lenses, although it was interrupted by the melt event in 2019.

4.5 Assessment of LeW time series in relation to firn property variations

Figure 8 shows the monthly mean LeW, MAR density, IMAU-FDM density, and normalised FAC time series along the transect highlighted in Fig. 3. The most significant reduction in LeW in Fig. 8a aligns with the sharp decrease in 2012, also shown in Fig. 7.

https://doi.org/10.5194/egusphere-2024-3251
Preprint. Discussion started: 13 November 2024

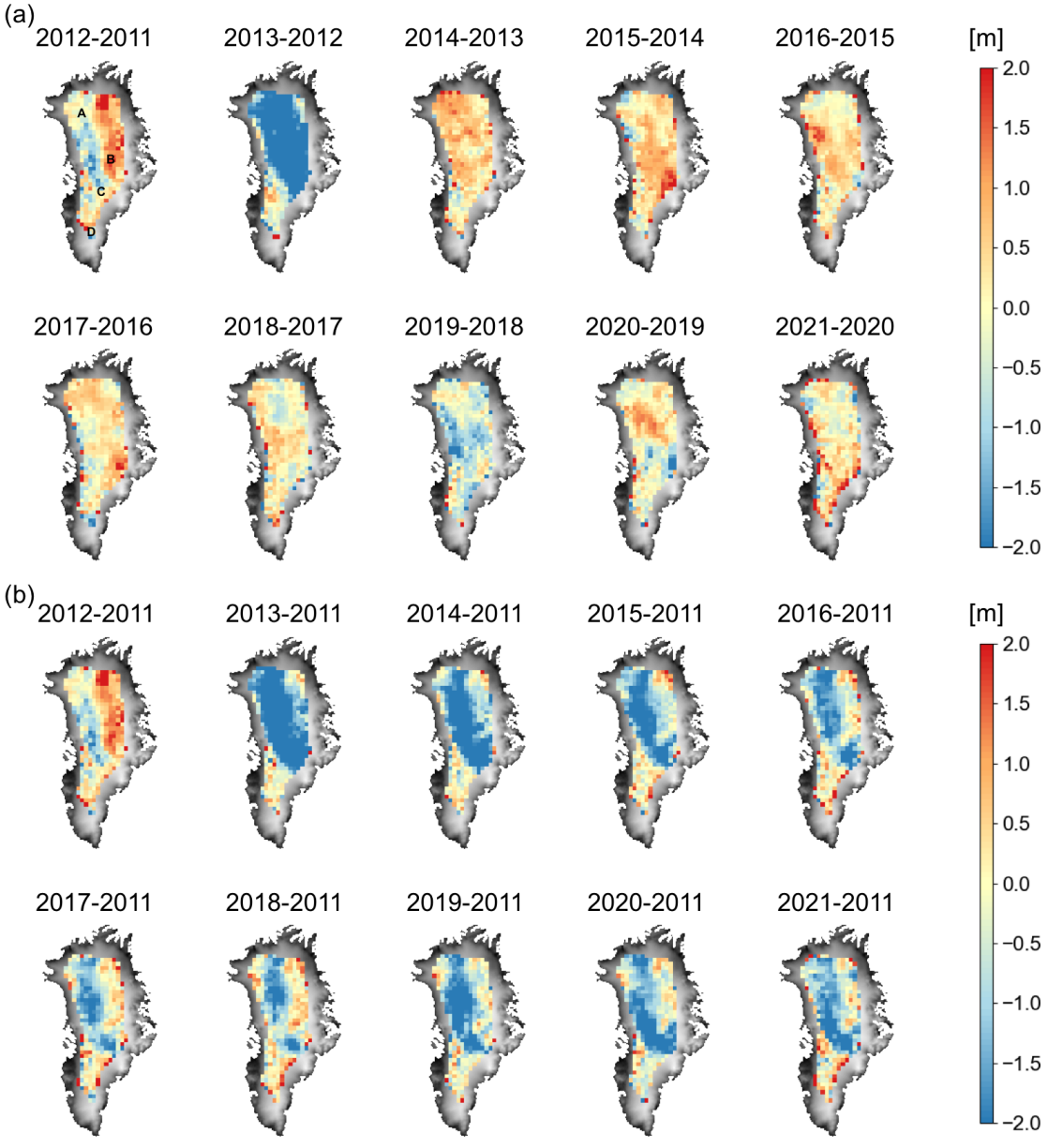

Figure 7. (a) Difference between the average LeW between January and May of every year and the average LeW between January and May of the previous year, and (b) difference between the average LeW between January and May of every year and the average LeW between January and May of 2011. Pixels A–D are labelled in the upper-left panel of (a).

https://doi.org/10.5194/egusphere-2024-3251
Preprint. Discussion started: 13 November 2024

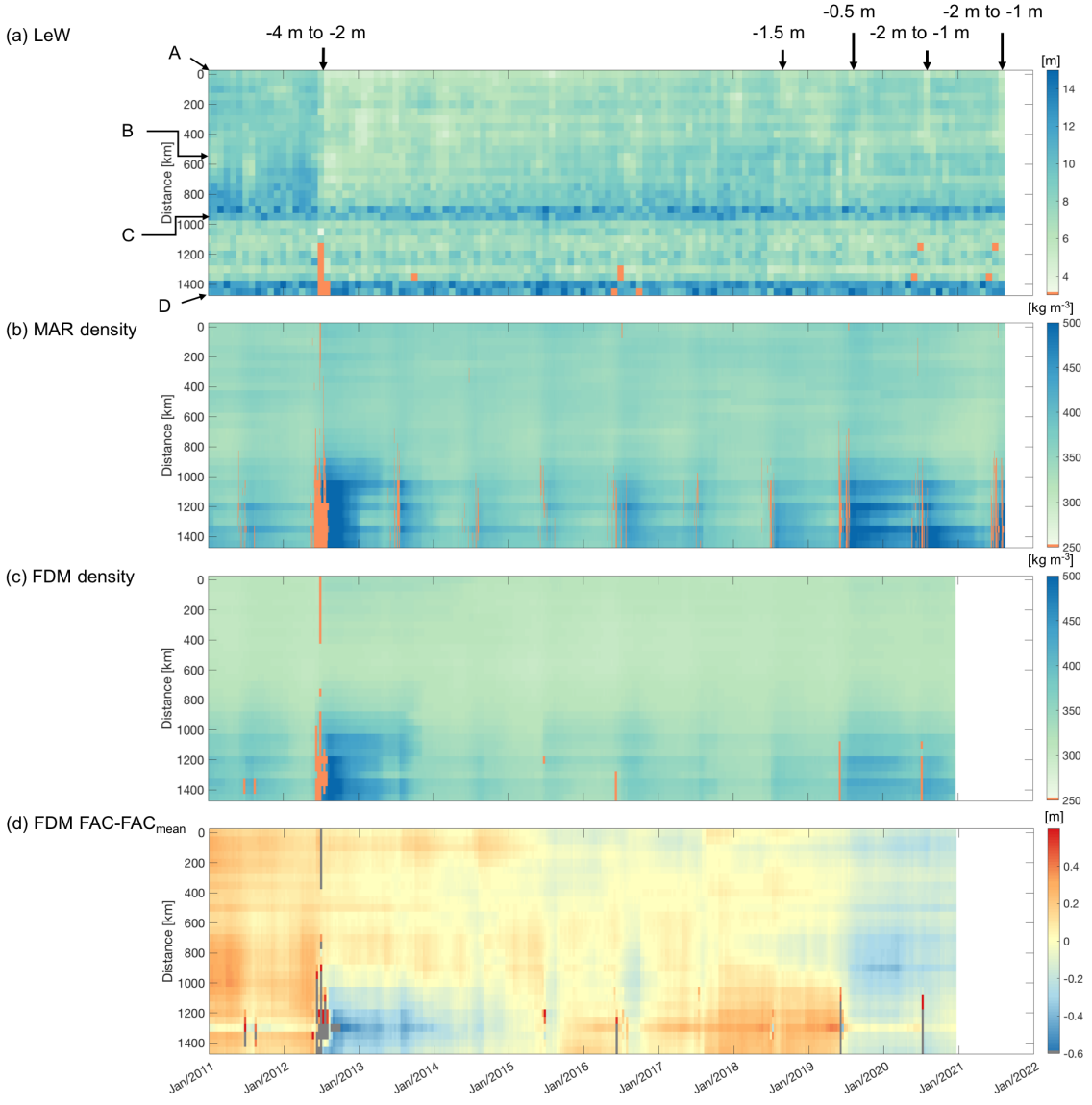

Figure 8. Monthly mean LeW, daily MAR density of the 1^{st} 1.5 m of snow, 10-day IMAU-FDM density, and IMAU-FDM firn air content (FAC) time series per pixel along the transect visualised in Fig. 3. The FAC time series are normalised with respect to the long-term mean of each pixel. The y-axes refer to the distance from the northernmost pixel. Arrows indicate the inspected pixels A–D. Large LeW decreases with respect to the previous month (exceeding 0.5 m) for pixels north of pixel C are labelled. Orange (a–c) or grey (d) colour indicates the values that are not available.

https://doi.org/10.5194/egusphere-2024-3251
Preprint. Discussion started: 13 November 2024

In the pixels north of pixel C, the monthly mean LeW is generally high (above 8 m) before the 2012 melt event, after which it abruptly drops below 6 m and gradually recovers until 2018. Along with the LeW reduction in 2012, both the MAR and IMAU-FDM models show increased average densities in the upper 1.5 m due to refreezing (Fig. A1c). Since 2018, LeW has fluctuated around 8 m, with annual drops occurring each summer from 2018 to 2021. Although these yearly declines are not as prolonged as in 2012, they occur more frequently than before 2018. Additionally, in 2019, the normalised FAC in these regions drops by approximately 0.1 m and remains lower than pre-2019 levels. The density also increases, remaining higher than both (i) pre-2012 levels and (ii) levels between 2014 and 2019. These observations align with Fig. 7, which shows that LeW in the interior of the ice sheet dropped after the 2012 melt event, gradually recovered between 2014 and 2019, and stabilised between 2019 and 2021, remaining about 2 m below 2011 levels.

In the pixels south of pixel C, the monthly mean LeW since 2011 does not show significant anomalies related to melt events (Fig. A1b). These pixels experience recurrent melting each year, as indicated by the density time series, which increase every summer. Densities in the southern pixels are also 10 $kg\ m^{-3}$ to 60 $kg\ m^{-3}$ higher than those in the north, and the drop-and-recovery pattern of FAC is more pronounced in the south. Additionally, the regions around pixel C and pixel D exhibit consistently higher LeW values (greater than 12 m) than those between pixels C and D (6 m to 8 m).

Our interpretation of the LeW patterns suggests that in the region between pixels A and C, the snow was initially dry before the 2012 melt, resulting in LeW patterns dominated by large volume scattering. The 2012 melt and the subsequent refreezing reduced volume scattering, causing a drop in LeW. LeW gradually recovered as the refrozen layer was buried, leading to the restoration of volume scattering. However, this recovery was interrupted by more recent and frequent melt events. In contrast, the regions south of pixel C show relatively stable LeW throughout the time series, as the melt–refreeze cycle occurs annually, causing less dramatic changes in volume scattering. Finally, the high LeW around pixels C and D is likely due to increased surface scattering caused by surface roughness and topography (Legrésy and Rémy, 1997), as discussed earlier in Section 4.2.

Figure 9 shows the variations in LeW, MAR density, IMAU-FDM density, and IMAU-FDM FAC (normalised relative to the long-term mean) between January 2011 and August 2021 for different elevation groups. In the low-elevation regions (below 1800 m), the LeW remains consistently high (around 20 m), with seasonal fluctuations of approximately 2 m during several years. For example, LeW decreases by about 2 m between June and August in 2013, 2014, 2015, 2018, and 2019. The density in these low-elevation areas also remains higher than in other parts of Greenland, with noticeable seasonal variations (densities increase in June). These density increases coincide with annual decreases in normalised FAC between June and August which correspond to the melt season.

Above the 1800 m elevation, a reduction in LeW is observed across all elevation groups following the 2012 melt event. The reduction is approximately 2 m in the 1800 m–2200 m elevation range, and approximately 5 m in regions above 2200 m. This LeW reduction in mid-2012 corresponds to the widespread melting, increased densities in both MAR and IMAU-FDM models, and a decline in normalised FAC. Smaller increases in density and decreases in FAC were also observed in mid-2015, mid-2016, and mid-2019 above 1800 m, with a slight decline in LeW during mid-2016 and mid-2018.

From the time series, we also observe that in the 1800 m–2200 m range, the LeW recovery rate is faster than in regions above 2200 m (approximately 0.6 $m\ yr^{-1}$ versus 0.2 $m\ yr^{-1}$). By spring 2018, in areas above 1800 m, the LeW had nearly

https://doi.org/10.5194/egusphere-2024-3251
Preprint. Discussion started: 13 November 2024

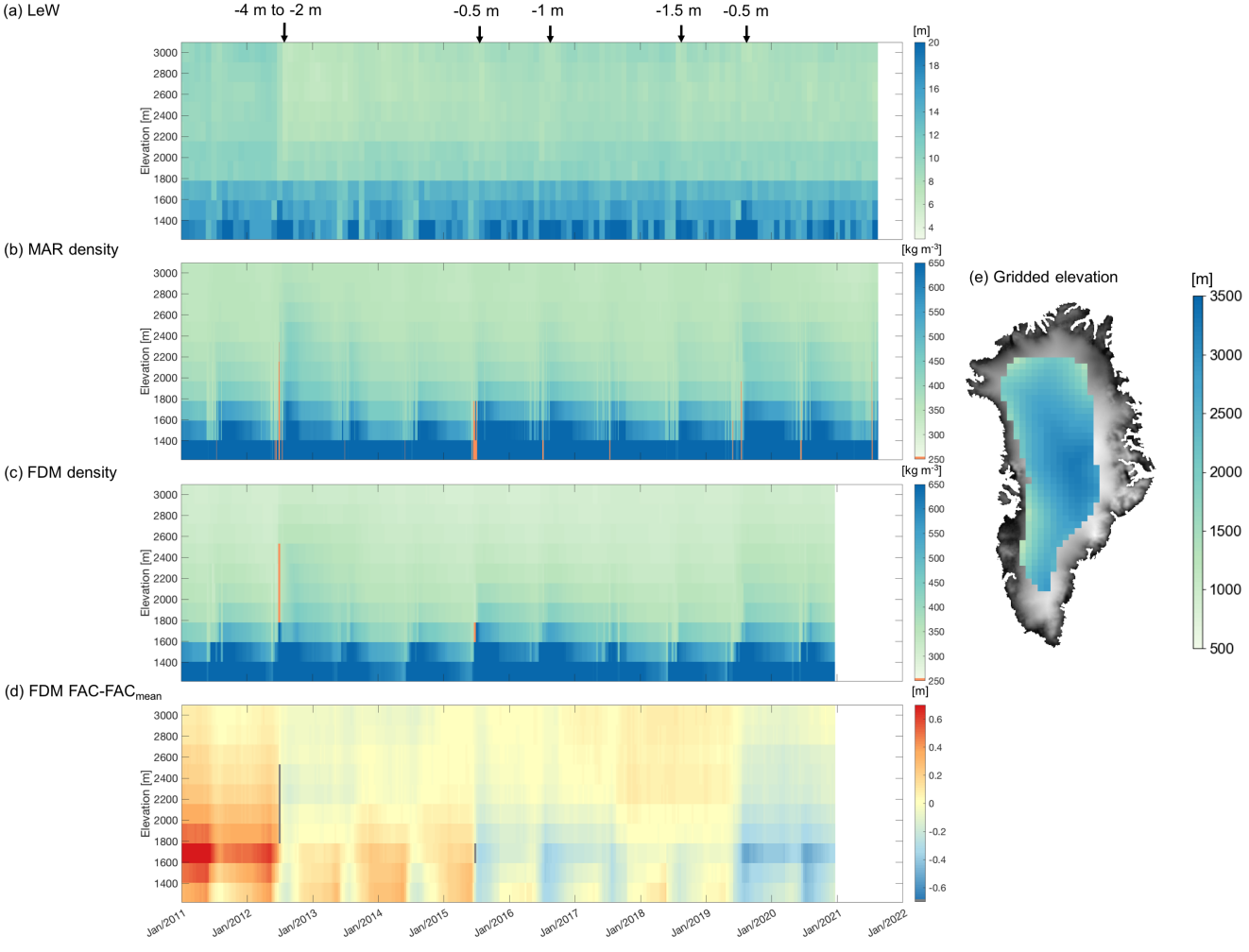

Figure 9. Time series of monthly mean LeW, daily density from MAR, 10-day resolution density from IMAU-FDM, and normalised FAC from IMAU-FDM, grouped by a down-sampled (gridded) DEM. Orange (a–c) or grey (d) colour indicates that the data are not available. A map of the gridded DEM is provided on the right, with the 1 km $\times$1 km Helm et al. (2014b) DEM as background.

https://doi.org/10.5194/egusphere-2024-3251
Preprint. Discussion started: 13 November 2024

returned to pre-2012 levels (about 1 m lower). However, it temporarily dropped in mid-2018 by about 1.5 m and has since fluctuated around that level. This trend is consistent with the observations in Fig. 7b. Notably, our time series indicates that aside from the well-documented 2019 melt event (Tedesco and Fettweis, 2020) (characterised by density increases and FAC decreases), a change in volume scattering already occurred in mid-2018. This led to a slight decrease in LeW above 2200 m, suggesting reduced volume scattering. However, unlike other events, the LeW decrease in mid-2018 does not correspond to a density increase or FAC decrease in the models.

Finally, Fig. 10 displays the IMAU-FDM density and normalised FAC time series from 1961 to 2020 for different elevation groups, alongside CryoSat-2 LeW data from the past decade. This comparison aims to determine whether the changes in volume scattering observed in CryoSat-2 LeW show a recent instability in Greenland's firn. Below 2800 m, densities have increased by 5 $kg\ m^{-3}$ to 20 $kg\ m^{-3}$ since 2012, while regions above 2800 m show only a slight increase (by about 3 $kg\ m^{-3}$) over the same period. In the past decade, FAC below 2200 m dropped significantly compared to earlier periods. In contrast, FAC values above 2200 m in the past decade are similar to those observed between 1975 and 1985, although they are lower than FAC values between 1985 and 2010. Additionally, between 2011 and 2020, FAC experienced slight drops and recoveries that correspond to the LeW pattern between 2012 and 2018, followed by another decline between 2018 and 2020, which also aligns with LeW trends.

5 Discussion

This study explores the capability of using LeW derived from CryoSat-2 waveforms to assess the spatial and temporal variations of the volume scattering properties of firn in Greenland. By comparing the LeW time series with the vertical stratigraphy from Rutishauser et al. (2024), we observed a slower recovery of firn following the 2012 melt event in the interior dry snow zone of Greenland compared to their findings. This discrepancy is likely due to LeW's focus on volume scattering, which contrasts with the limitations of dz in accounting for topography, roughness, and timing corrections of the MCoRDS signal, as noted by Rutishauser et al. (2024). Our findings suggest that CryoSat-2 LeW, with its greater sensitivity to volume scattering, provides a more reliable tool for assessing firn recovery in the dry snow zone, where surface scattering is minimal. Furthermore, the spatial and temporal continuity offered by CryoSat-2 is a significant advantage over Operation IceBridge (OIB) data, which is more spatially limited. CryoSat-2's Greenland-wide coverage enables a more comprehensive tracking of firn evolution, particularly in remote regions where OIB data may not be available, providing a more detailed overview of post-melt firn processes.

However, outside of the central dry snow zones, LeW is less effective in tracking melt–refreeze processes, as surface features such as roughness and topography begin to dominate its variability. This was confirmed through comparisons with ArcticDEM, firn models, and the data from Scanlan et al. (2023). To further validate LeW as a measure of firn changes, we compared it with CryoSat-2 penetration depth (calculated as the height difference between ICESat-2 and CryoSat-2). Overall, the relationship is similar to the conclusion of Michel et al. (2014), who proposed a linear function between LeW and penetration depth in flat regions of Antarctica. Our study, although not explicitly defining a "flat" region, delineated the interior of Greenland where the correlation between LeW and penetration depth is positive (around 0.3) and is significant ($p \leq 0.05$). By distinguishing

https://doi.org/10.5194/egusphere-2024-3251
Preprint. Discussion started: 13 November 2024

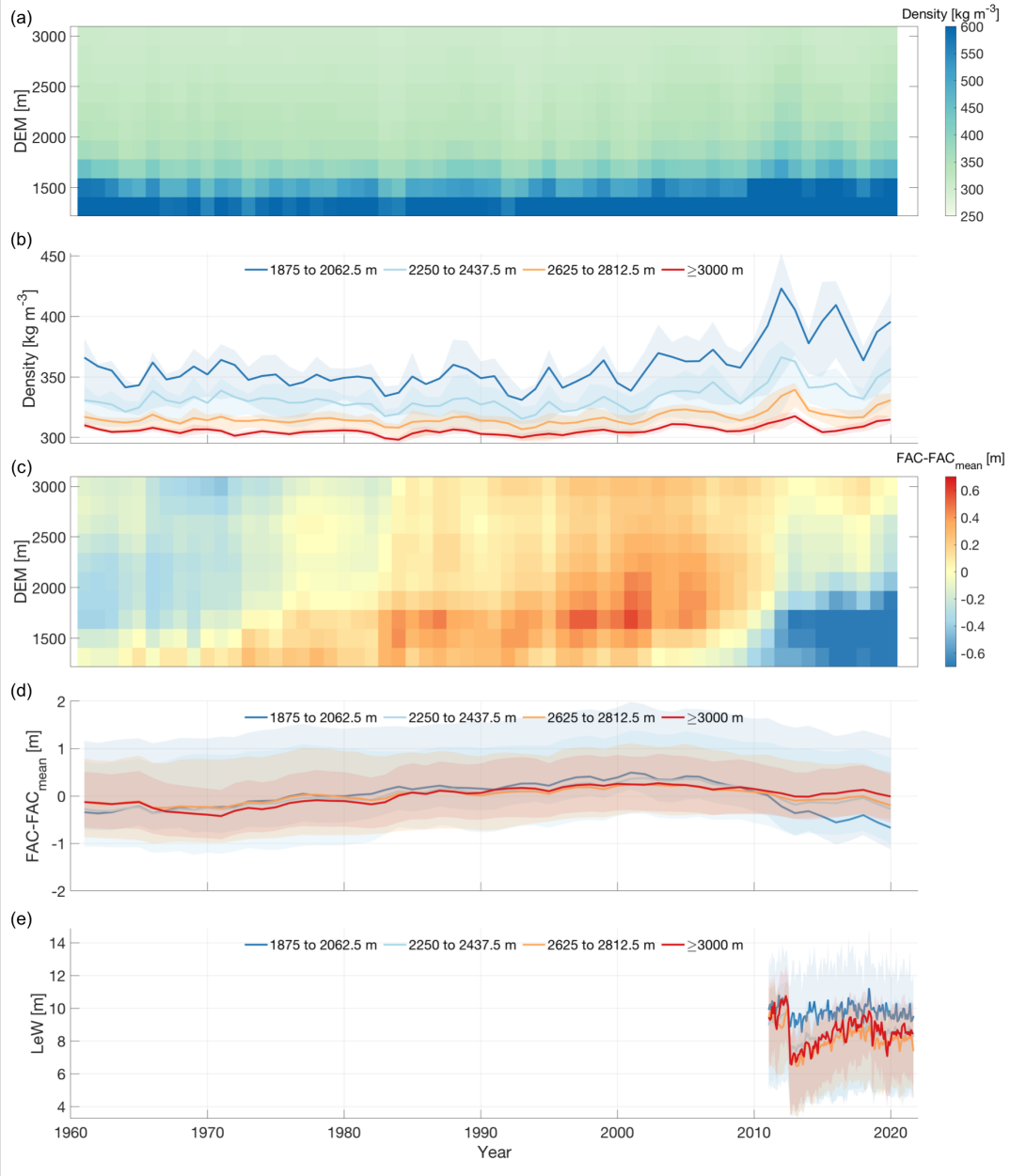

Figure 10. (a) Annual mean density between 1961 and 2020 from IMAU-FDM, grouped by gridded DEM. (b) Density variation between 1961 and 2020 for selected gridded DEM groups; the annual mean densities are in solid lines and the 25–75th percentiles are shaded. (c) Annual mean FAC between 1961 and 2020 from IMAU-FDM, normalised by long-term mean of FAC for visualisation. (d) Normalised FAC between 1961 and 2020 for selected gridded DEM groups; the annual mean densities are in solid lines and the 25–75th percentiles are shaded. (e) CryoSat-2 LeW between 2011 and 2021 for selected gridded DEM groups; the monthly mean densities are in solid lines and the 25–75th percentiles are shaded.

https://doi.org/10.5194/egusphere-2024-3251
Preprint. Discussion started: 13 November 2024

areas where LeW is dominated by volume scattering from those dominated by surface scattering, our study provides a valuable framework for understanding firn response to melt events across different regions of Greenland.

This study is the first known demonstration of a Greenland-wide (within the CryoSat-2 LRM data coverage) LeW time series analysis, supported by two different firn models. The time series between 2011 and 2021 show that the 2012 melt event had a more prolonged impact than any other following melt events, resulting in a reduction in LeW that persisted until 2018, especially over the central-west Greenland. Recurrent melt events since 2018 have interrupted the firn recovery that was expected by Nilsson et al. (2015), underscoring the importance of monitoring these processes over long timescales. These findings highlight the value of CryoSat-2 LeW in assessing post-melt firn evolution, particularly at higher elevations.

When observed over a longer time scale (between 1960 and 2020), firn models indicate that the most pronounced firn changes, such as increases in density and decreases in FAC, occur below 1800 m elevation. At these lower elevations, LeW changes are less pronounced, showing only a 2 m reduction. In contrast, at elevations above 2250 m, LeW is comparably sensitive to the long-term effect of refreezing layer as FAC and density, while exhibiting higher sensitivity in 2018. This sensitivity suggests that LeW data could play a crucial role in refining firn models, especially for higher elevations, where existing models may underestimate the impacts of melt events on volume scattering.

Our findings indicate that in southern and low-elevation regions of Greenland, where surface scattering dominates and melt events are more frequent, LeW is less effective in capturing firn changes. Future studies could address these limitations by incorporating additional altimeter-derived parameters such as trailing edge slope (TeS), waveform peakiness, and backscatter coefficients, which are more sensitive to surface scattering processes (Nilsson et al., 2015). These parameters, combined with LeW, would offer a more complete picture of surface and volume scattering interactions.

To better simulate the complex contributions of surface and volume scattering, radiative transfer models (Adodo et al., 2018; Larue et al., 2021) can be employed. These models, when taking into account the varying viewing geometry of the satellite, can enable more accurate representations of how melt–refreeze processes (characterised by varying temperature, firn density, microstructure and grain size) impact firn properties.

The ongoing ICESat-2 mission should also continue to provide the opportunity to derive Ku-band radar penetration depth, which also allows to continuously monitor changes in sub-surface firn due to melt–refreeze processes. This could complement CryoSat-2 data, offering a higher-resolution view of firn structure over time. Additionally, combining radar altimeter data from different frequencies can help derive volume scattering information from different subsurface layers, as suggested by Adodo et al. (2018), Otosaka et al. (2020), and Scanlan et al. (2023). This multi-layered approach can be particularly useful in regions where surface and volume scattering overlap, offering more nuanced insights into firn changes.

To enhance future firn studies, LeW data can be integrated into firn models to improve predictions of melt impacts on volume scattering, particularly at higher elevations. By using interdisciplinary approaches, we can deepen our understanding of how melt events affect firn properties over the long term, improving our ability to predict future ice sheet dynamics.

https://doi.org/10.5194/egusphere-2024-3251
Preprint. Discussion started: 13 November 2024

6 Conclusions

This study explored and demonstrated the possibility for using the LeW derived by CryoSat-2 to assess spatio-temporal changes in Greenland firn status caused by melt–refreezing events. While previous studies indicated a recovery pattern in LeW when new snow is deposited on top of the refrozen layers, our study further investigated whether this process can be observed with the help of LeW time series. Our analysis showed that the recovery speed can be related to the elevation and new snow deposition. However, the recovery is hampered by more recent melt events (although not as severe as the 2012 event). In central-west Greenland, the LeW never recovered to the pre-2012 level; in regions where LeW managed to recover, new melt events resulted in new LeW reductions, which indicates a reduction in volume scattering hence a reduction in its capacity to store meltwater. Such alternation can also be confirmed using the long-term time series, which showed a decreasing LeW, an elevated density and a decreasing FAC in recent decades. This correspondence between the reduction in volume scattering and the reduction in FAC confirms that the more frequent melt events reduce the capability of Greenland firn to retain meltwater, and in turn may result in an accelerated runoff from the ice sheet (Vandecrux et al., 2019).

Finally, this study has demonstrated the reliability and limitations for using LeW from radar altimeter to understand the volume scattering variations and associated firn processes, paving the way for the study of sub-surface firn processes in a changing climate. The use of a combination of CryoSat-2 and ICESat-2 height measurements can also contribute to the study of Ku-band penetration depth hence volume scattering.

Code and data availability. Software for the in-house processing of CryoSat-2 data from L1b to L2 is available on request from Cornelis Slobbe. The MAR datasets are available on request from Xavier Fettweis. The IMAU-FDM datasets are available on request from Max Brils. ArcticDEM is provided by the Polar Geospatial Center under NSF-OPP awards 1043681, 1559691, and 1542736. The DEM of Greenland used for result visualisation is provided by Helm et al. (2014a, b) under license Creative Commons Attribution 3.0 Unported. The CryoSat-2 L1b and L2I data are provided online by ESA and the ICESat-2 L3A data are provided online by NSIDC (https://nsidc.org/data/atl06). The OIB-derived vertical trstigraphy dataset is available on https://doi.org/10.22008/FK2/OLVPFG. The surface roughness data is available on https://doi.org/10.11583/DTU.21333291.v1.

Appendix A: LeW and MAR melt, refreeze and total snow height time series

Figure A1 illustrates the time series of monthly mean LeW, MAR meltwater production, meltwater refreezing and accumulated total snow height change along the transect highlighted in Fig. 3. The meltwater production and refreezing correspond to the density increases in Fig. 8b. Figure A1a indicates that the overall decrease in LeW in 2012 corresponds to both the extensive meltwater production as well as refreezing. Furthermore, a slight LeW decrease in mid-2019 between pixels A and C also corresponds with the melt–refreezing event. By comparing Fig. A1a and Fig. A1d, we notice that north of pixel B shows a slower LeW recovery than between pixels B and C, which corresponds to a lower cumulative total snow height change (i.e snowfall accumulation) from the 12th of July 2012.

https://doi.org/10.5194/egusphere-2024-3251
Preprint. Discussion started: 13 November 2024

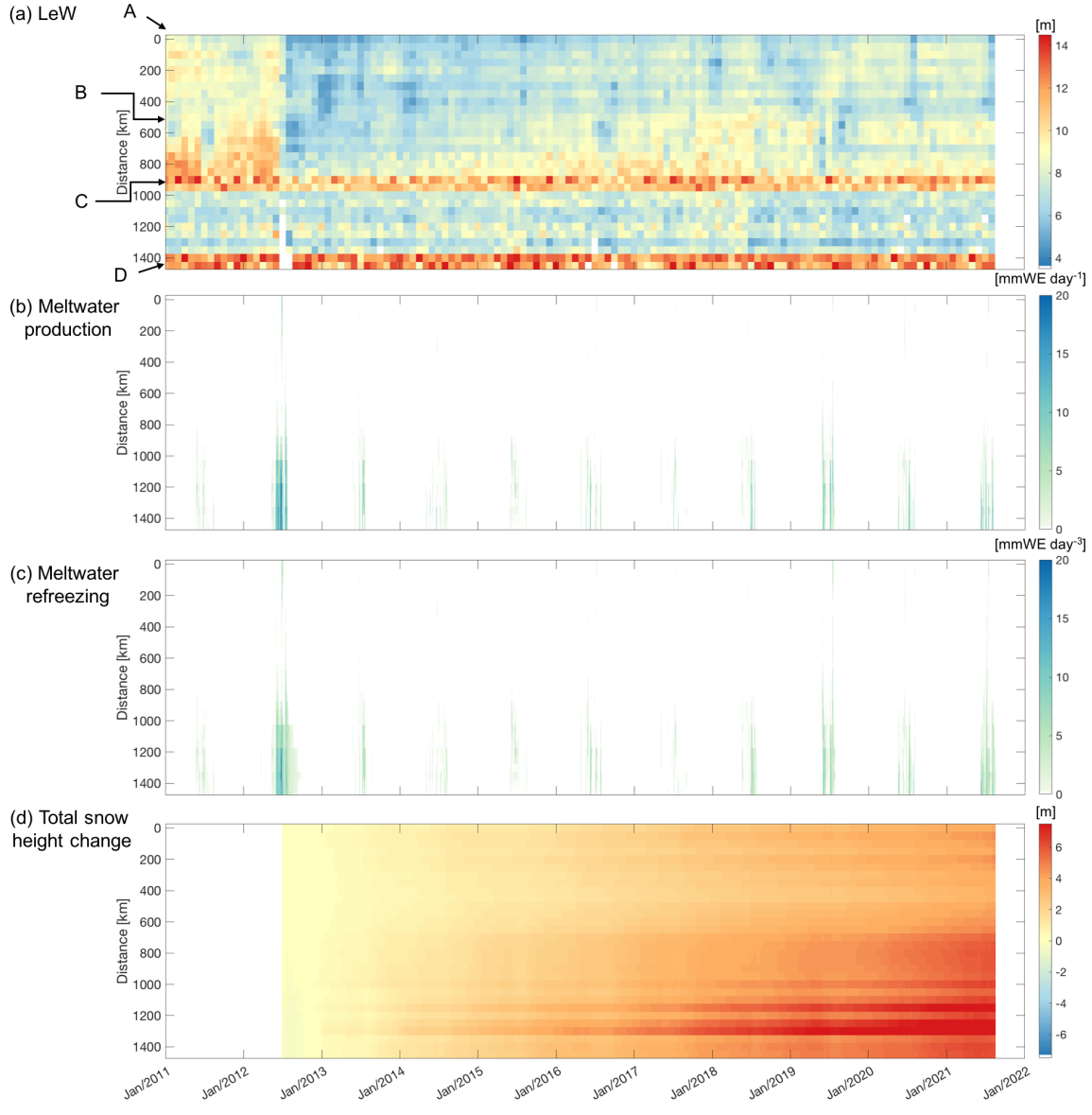

Figure A1. Monthly mean LeW, daily MAR surface meltwater production, daily MAR meltwater refreezing, and daily accumulated total snow height change (i.e. snow accumulation) from 12 July 2012 time series per pixel along the transect visualised in Fig. 3. The LeW and MAR total snow height change time series adopt a diverging colour bar to enhance the contrast. The y-axes refer to the distance from the northernmost pixel. White colour indicates the values that are not available. Arrows indicate the inspected pixels A—D.

https://doi.org/10.5194/egusphere-2024-3251
Preprint. Discussion started: 13 November 2024

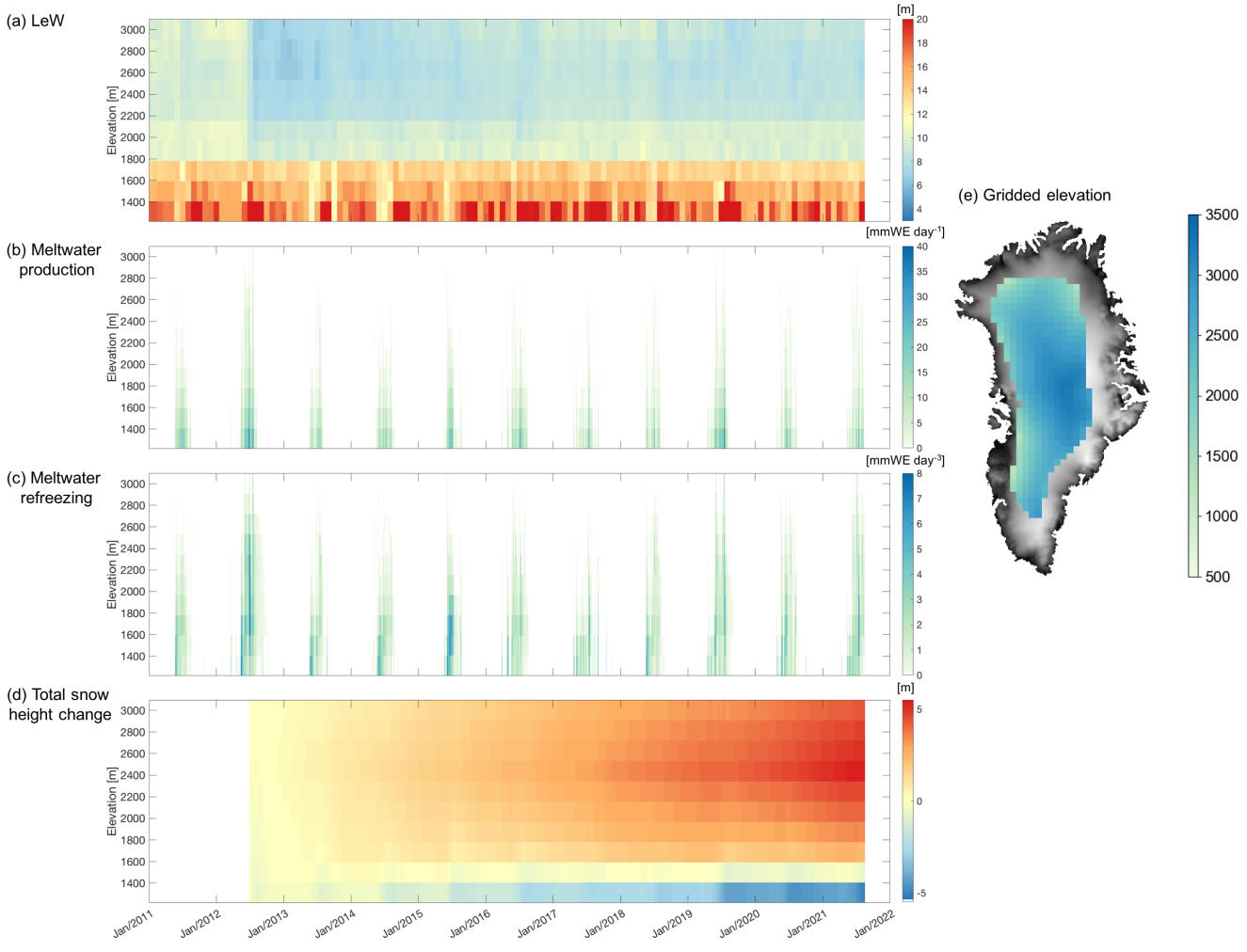

Figure A2. Monthly mean LeW, daily MAR surface meltwater production, daily meltwater refreezing, and daily accumulated total snow height change (i.e. snow accumulation) from July 2012 time series grouped by a down-sampled (gridded) DEM. The LeW and MAR total snow height change time series adopt a diverging colour bar to enhance the contrast. White colour indicates that the data are not available. A map of the gridded DEM is provided on the right, with the 1 km $\times$1 km Helm et al. (2014b) DEM as background.

https://doi.org/10.5194/egusphere-2024-3251
Preprint. Discussion started: 13 November 2024

Similarly, we present the time series per elevation group in Fig. A2. The melt–refreeze patterns correspond with the density increases in Fig. 9b. However, differently from Fig. A1a and Fig. A1d, Fig. A2a and Fig. A2d do not show a high correspondence between LeW recovery and total accumulated snow: the total accumulated snow height from 12 July 2012 shows the highest increase between 2014 and 2021 at around 2400 m elevation, while the fastest LeW recovery occurs between 1800 m and 2200 m. This discrepancy could be attributed to the significantly larger snow accumulation in the South of Greenland than the North, despite being at the same elevation.

Author contributions. WL, SL and BW designed the study. WL conducted data management, processing, and analysis; produced the figures; and provided the manuscript with contributions from the other co-authors. SL provided support on data visualisation and analysis. BW provided expertise for data analysis. CS provided expertise and software for radar altimetry processing and data analysis. XF generated the MAR outputs. MB generated the IMAU-FDM outputs.

Competing interests. Stef Lhermitte, Bert Wouters and Xavier Fettweis are members of the editorial board of The Cryosphere.

Acknowledgements. The research is supported by the Dutch Research Council (NWO) through the ALWGO.2017.033 project. ArcticDEM is provided by the Polar Geospatial Center under NSF-OPP awards 1043681, 1559691, and 1542736. The DEM of Greenland used for result visualisation is provided by Helm et al. (2014a, b) under license Creative Commons Attribution 3.0 Unported.
ChatGPT is used for language checks in parts of the manuscript.

https://doi.org/10.5194/egusphere-2024-3251
Preprint. Discussion started: 13 November 2024

References

Abdalati, W., Zwally, H. J., Bindschadler, R., Csatho, B., Farrell, S. L., Fricker, H. A., Harding, D., Kwok, R., Lefsky, M., Markus, T., et al.: The ICESat-2 laser altimetry mission, Proceedings of the IEEE, 98, 735–751, 2010.

Adodo, F. I., Remy, F., and Picard, G.: Seasonal variations of the backscattering coefficient measured by radar altimeters over the Antarctic Ice Sheet, The Cryosphere, 12, 1767–1778, https://doi.org/10.5194/tc-12-1767-2018, 2018.

Alley, K., Scambos, T., Miller, J., Long, D., and MacFerrin, M.: Quantifying vulnerability of Antarctic ice shelves to hydrofracture using microwave scattering properties, Remote Sensing of Environment, 210, 297–306, https://doi.org/10.1016/j.rse.2018.03.025, 2018.

Bamber, J. L.: Ice sheet altimeter processing scheme, International Journal of Remote Sensing, 15, 925–938, https://doi.org/10.1080/01431169408954125, 1994.

Bermudez-Edo, M., Barnaghi, P., and Moessner, K.: Analysing real world data streams with spatio-temporal correlations: Entropy vs. Pearson correlation, Automation in Construction, 88, 87–100, https://doi.org/10.1016/j.autcon.2017.12.036, 2018.

Brils, M., Kuipers Munneke, P., van de Berg, W. J., and van den Broeke, M.: Improved representation of the contemporary Greenland ice sheet firn layer by IMAU-FDM v1.2G, Geoscientific Model Development, 15, 7121–7138, https://doi.org/10.5194/gmd-15-7121-2022, 2022.

Castelao, R. M. and Medeiros, P. M.: Coastal Summer Freshening and Meltwater Input off West Greenland from Satellite Observations, Remote Sensing, 14, 6069, https://doi.org/10.3390/rs14236069, 2022.

Davis, C.: A robust threshold retracking algorithm for measuring ice-sheet surface elevation change from satellite radar altimeters, IEEE Transactions on Geoscience and Remote Sensing, 35, 974–979, https://doi.org/10.1109/36.602540, 1997.

European Space Agency: L1b LRM Precise Orbit. Baseline D, https://doi.org/10.5270/CR2-cbow23i, (last access: 17 Semptember 2022), 2019.

Fahnestock, M., Bindschadler, R., Kwok, R., and Jezek, K.: Greenland Ice Sheet Surface Properties and Ice Dynamics from ERS-1 SAR Imagery, Science, 262, 1530–1534, https://doi.org/10.1126/science.262.5139.1530, 1993.

Fettweis, X., Tedesco, M., van den Broeke, M., and Ettema, J.: Melting trends over the Greenland ice sheet (1958–2009) from spaceborne microwave data and regional climate models, The Cryosphere, 5, 359–375, https://doi.org/10.5194/tc-5-359-2011, 2011.

Fettweis, X., Box, J. E., Agosta, C., Amory, C., Kittel, C., Lang, C., van As, D., Machguth, H., and Gallée, H.: Reconstructions of the 1900–2015 Greenland ice sheet surface mass balance using the regional climate MAR model, The Cryosphere, 11, 1015–1033, https://doi.org/10.5194/tc-11-1015-2017, 2017.

Gommenginger, C., Thibaut, P., Fenoglio-Marc, L., Quartly, G., Deng, X., Gómez-Enri, J., Challenor, P., and Gao, Y.: Retracking Altimeter Waveforms Near the Coasts, in: Coastal Altimetry, pp. 61–101, Springer Berlin Heidelberg, https://doi.org/10.1007/978-3-642-12796-0_4, 2010.

Hall, D., Box, J., Casey, K., Hook, S., Shuman, C., and Steffen, K.: Comparison of satellite-derived and in-situ observations of ice and snow surface temperatures over Greenland, Remote Sensing of Environment, 112, 3739–3749, https://doi.org/10.1016/j.rse.2008.05.007, 2008.

Harper, J., Humphrey, N., Pfeffer, W. T., Brown, J., and Fettweis, X.: Greenland ice-sheet contribution to sea-level rise buffered by meltwater storage in firn, Nature, 491, 240–243, https://doi.org/10.1038/nature11566, 2012.

Heilig, A., Eisen, O., MacFerrin, M., Tedesco, M., and Fettweis, X.: Seasonal monitoring of melt and accumulation within the deep percolation zone of the Greenland Ice Sheet and comparison with simulations of regional climate modeling, The Cryosphere, 12, 1851–1866, https://doi.org/10.5194/tc-12-1851-2018, 2018.

https://doi.org/10.5194/egusphere-2024-3251
Preprint. Discussion started: 13 November 2024

Helm, V., Humbert, A., and Miller, H.: Elevation and elevation change of Greenland and Antarctica derived from CryoSat-2, The Cryosphere, 8, 1539–1559, https://doi.org/10.5194/tc-8-1539-2014, 2014a.

Helm, V., Humbert, A., and Miller, H.: Elevation Model of Greenland derived from CryoSat-2 in the period 2011 to 2013, links to DEM and uncertainty map as GeoTIFF, https://doi.org/10.1594/PANGAEA.831393, 2014b.

Huybrechts, P., Goelzer, H., Janssens, I., Driesschaert, E., Fichefet, T., Goosse, H., and Loutre, M.-F.: Response of the Greenland and Antarctic Ice Sheets to Multi-Millennial Greenhouse Warming in the Earth System Model of Intermediate Complexity LOVECLIM, Surveys in Geophysics, 32, 397–416, https://doi.org/10.1007/s10712-011-9131-5, 2011.

Koenig, L. S., Ivanoff, A., Alexander, P. M., MacGregor, J. A., Fettweis, X., Panzer, B., Paden, J. D., Forster, R. R., Das, I., McConnell, J. R., Tedesco, M., Leuschen, C., and Gogineni, P.: Annual Greenland accumulation rates (2009–2012) from airborne snow radar, The Cryosphere, 10, 1739–1752, https://doi.org/10.5194/tc-10-1739-2016, 2016.

Kuipers Munneke, P., Ligtenberg, S. R., Suder, E. A., and Van den Broeke, M. R.: A model study of the response of dry and wet firn to climate change, Annals of Glaciology, 56, 1–8, https://doi.org/10.3189/2015aog70a994, 2015.

Lambin, C., Fettweis, X., Kittel, C., Fonder, M., and Ernst, D.: Assessment of future wind speed and wind power changes over South Greenland using the Modèle Atmosphérique Régional regional climate model, International Journal of Climatology, 43, 558–574, https://doi.org/10.1002/joc.7795, 2022.

Larue, F., Picard, G., Aublanc, J., Arnaud, L., Robledano-Perez, A., Meur, E. L., Favier, V., Jourdain, B., Savarino, J., and Thibaut, P.: Radar altimeter waveform simulations in Antarctica with the Snow Microwave Radiative Transfer Model (SMRT), Remote Sensing of Environment, 263, 112 534, https://doi.org/10.1016/j.rse.2021.112534, 2021.

Legrésy, B. and Rémy, F.: Altimetric observations of surface characteristics of the Antarctic ice sheet, Journal of Glaciology, 43, 265–275, https://doi.org/10.3189/s002214300000321x, 1997.

Lenton, T. M., Held, H., Kriegler, E., Hall, J. W., Lucht, W., Rahmstorf, S., and Schellnhuber, H. J.: Tipping elements in the Earth's climate system, Proceedings of the National Academy of Sciences, 105, 1786–1793, https://doi.org/10.1073/pnas.0705414105, 2008.

Li, W., Slobbe, C., and Lhermitte, S.: A leading-edge-based method for correction of slope-induced errors in ice-sheet heights derived from radar altimetry, The Cryosphere, 16, 2225–2243, https://doi.org/10.5194/tc-16-2225-2022, 2022.

Machguth, H., MacFerrin, M., van As, D., Box, J. E., Charalampidis, C., Colgan, W., Fausto, R. S., Meijer, H. A. J., Mosley-Thompson, E., and van de Wal, R. S. W.: Greenland meltwater storage in firn limited by near-surface ice formation, Nature Climate Change, 6, 390–393, https://doi.org/10.1038/nclimate2899, 2016.

Meierbachtol, T., Harper, J., and Humphrey, N.: Basal Drainage System Response to Increasing Surface Melt on the Greenland Ice Sheet, Science, 341, 777–779, https://doi.org/10.1126/science.1235905, 2013.

Meloni, M., Bouffard, J., Parrinello, T., Dawson, G., Garnier, F., Helm, V., Bella, A. D., Hendricks, S., Ricker, R., Webb, E., Wright, B., Nielsen, K., Lee, S., Passaro, M., Scagliola, M., Simonsen, S. B., Sørensen, L. S., Brockley, D., Baker, S., Fleury, S., Bamber, J., Maestri, L., Skourup, H., Forsberg, R., and Mizzi, L.: CryoSat Ice Baseline-D validation and evolutions, The Cryosphere, 14, 1889–1907, https://doi.org/10.5194/tc-14-1889-2020, 2020.

Michel, A., Flament, T., and Rémy, F.: Study of the Penetration Bias of ENVISAT Altimeter Observations over Antarctica in Comparison to ICESat Observations, Remote Sensing, 6, 9412–9434, https://doi.org/10.3390/rs6109412, 2014.

National Snow and Ice Data Center (NSIDC): ATL06 release 005 known issues, https://nsidc.org/sites/nsidc.org/files/technical-references/ICESat2_ATL06_Known_Issues_v005.pdf, [Date accessed: 18 April, 2022], 2021.

https://doi.org/10.5194/egusphere-2024-3251
Preprint. Discussion started: 13 November 2024

Nghiem, S. V., Hall, D. K., Mote, T. L., Tedesco, M., Albert, M. R., Keegan, K., Shuman, C. A., DiGirolamo, N. E., and Neumann, G.: The extreme melt across the Greenland ice sheet in 2012, Geophysical Research Letters, 39, https://doi.org/10.1029/2012gl053611, 2012.

Nilsson, J., Vallelonga, P., Simonsen, S. B., Sørensen, L. S., Forsberg, R., Dahl-Jensen, D., Hirabayashi, M., Goto-Azuma, K., Hvidberg, C. S., Kjaer, H. A., and Satow, K.: Greenland 2012 melt event effects on CryoSat-2 radar altimetry, Geophysical Research Letters, 42, 3919–3926, https://doi.org/10.1002/2015gl063296, 2015.

Noh, M.-J. and Howat, I. M.: Automated stereo-photogrammetric DEM generation at high latitudes: Surface Extraction with TIN-based Search-space Minimization (SETSM) validation and demonstration over glaciated regions, GIScience & Remote Sensing, 52, 198–217, https://doi.org/10.1080/15481603.2015.1008621, 2015.

Noël, B., van de Berg, W. J., van Wessem, J. M., van Meijgaard, E., van As, D., Lenaerts, J. T. M., Lhermitte, S., Kuipers Munneke, P., Smeets, C. J. P. P., van Ulft, L. H., van de Wal, R. S. W., and van den Broeke, M. R.: Modelling the climate and surface mass balance of polar ice sheets using RACMO2 – Part 1: Greenland (1958–2016), The Cryosphere, 12, 811–831, https://doi.org/10.5194/tc-12-811-2018, 2018.

Otosaka, I. N.: Firn density profiles in West Central Greenland (ESA CryoVEx 2017), https://doi.org/10.1594/PANGAEA.921672, (last access: 27 October 2023), 2020.

Otosaka, I. N., Shepherd, A., Casal, T. G. D., Coccia, A., Davidson, M., Di Bella, A., Fettweis, X., Forsberg, R., Helm, V., Hogg, A. E., Hvidegaard, S. M., Lemos, A., Macedo, K., Kuipers Munneke, P., Parrinello, T., Simonsen, S. B., Skourup, H., and Sørensen, L. S.: Surface Melting Drives Fluctuations in Airborne Radar Penetration in West Central Greenland, Geophysical Research Letters, 47, https://doi.org/10.1029/2020gl088293, 2020.

Porter, C., Howat, I., Noh, M.-J., Husby, E., Khuvis, S., Danish, E., Tomko, K., Gardiner, J., Negrete, A., Yadav, B., Klassen, J., Kelleher, C., Cloutier, M., Bakker, J., Enos, J., Arnold, G., Bauer, G., and Morin, P.: ArcticDEM - Mosaics, Version 4.1, https://doi.org/10.7910/DVN/3VDC4W, 2023.

Rennermalm, Å. K., Hock, R., Covi, F., Xiao, J., Corti, G., Kingslake, J., Leidman, S. Z., Miège, C., Macferrin, M., Machguth, H., Osterberg, E., Kameda, T., and McConnell, J. R.: Shallow firn cores 1989–2019 in southwest Greenland's percolation zone reveal decreasing density and ice layer thickness after 2012, Journal of Glaciology, 68, 431–442, https://doi.org/10.1017/jog.2021.102, 2021.

Rutishauser, A., Scanlan, K. M., Vandecrux, B., Karlsson, N. B., Jullien, N., Ahlstrøm, A. P., Fausto, R. S., and How, P.: Mapping the vertical heterogeneity of Greenland's firn from 2011–2019 using airborne radar and laser altimetry, The Cryosphere, 18, 2455–2472, https://doi.org/10.5194/tc-18-2455-2024, 2024.

Sasgen, I., van den Broeke, M., Bamber, J. L., Rignot, E., Sørensen, L. S., Wouters, B., Martinec, Z., Velicogna, I., and Simonsen, S. B.: Timing and origin of recent regional ice-mass loss in Greenland, Earth and Planetary Science Letters, 333-334, 293–303, https://doi.org/10.1016/j.epsl.2012.03.033, 2012.

Scanlan, K. M., Rutishauser, A., and Simonsen, S. B.: Observing the Near-Surface Properties of the Greenland Ice Sheet, Geophysical Research Letters, 50, https://doi.org/10.1029/2022gl101702, 2023.

Schaller, C. F., Freitag, J., Kipfstuhl, S., Laepple, T., Steen-Larsen, H. C., and Eisen, O.: A representative density profile of the North Greenland snowpack, The Cryosphere, 10, 1991–2002, https://doi.org/10.5194/tc-10-1991-2016, 2016a.

Schaller, C. F., Freitag, J., Kipfstuhl, S., Laepple, T., Steen-Larsen, H. C., and Eisen, O.: NEEM to EGRIP traverse - density and δ^{18}O of the surface snow (2 m profiles), https://doi.org/10.1594/PANGAEA.867875, (last access: 13 December 2023), 2016b.

Simonsen, S. B. and Sørensen, L. S.: Implications of changing scattering properties on Greenland ice sheet volume change from Cryosat-2 altimetry, Remote Sensing of Environment, 190, 207–216, https://doi.org/10.1016/j.rse.2016.12.012, 2017.

https://doi.org/10.5194/egusphere-2024-3251
Preprint. Discussion started: 13 November 2024

Slater, T., Shepherd, A., McMillan, M., Muir, A., Gilbert, L., Hogg, A. E., Konrad, H., and Parrinello, T.: A new digital elevation model of Antarctica derived from CryoSat-2 altimetry, The Cryosphere, 12, 1551–1562, https://doi.org/10.5194/tc-12-1551-2018, 2018.

Smith, B., Fricker, H. A., Gardner, A., Siegfried, M. R., Adusumilli, S., Csathó, B. M., Holschuh, N., Nilsson, J., Paolo, F. S., and the ICESat-2 Science Team: ATLAS/ICESat-2 L3A Land Ice Height, Version 5, https://doi.org/10.5067/ATLAS/ATL06.005, (last access: 15 Semptember 2022), 2020.

Smith, B., Hancock, D., Harbeck, K., Roberts, L., Neumann, T., Brunt, K., Fricker, H., Gardner, A., Siegfried, M., Adusumilli, S., Csatho, B., Holschuh, N., Nilsson, J., Paolo, F., and Felikson, D.: Ice, Cloud, and Land Elevation Satellite (ICESat-2) Project Algorithm Theoretical Basis Document (ATBD) for Land Ice Along-Track Height Product (ATL06), version 6, https://doi.org/10.5067/VWOKQDYJ7ODB, 2023.

Smith, B. E., Gardner, A., Schneider, A., and Flanner, M.: Modeling biases in laser-altimetry measurements caused by scattering of green light in snow, Remote Sensing of Environment, 215, 398–410, https://doi.org/10.1016/j.rse.2018.06.012, 2018.

Sundal, A. V., Shepherd, A., Nienow, P., Hanna, E., Palmer, S., and Huybrechts, P.: Melt-induced speed-up of Greenland ice sheet offset by efficient subglacial drainage, Nature, 469, 521–524, https://doi.org/10.1038/nature09740, 2011.

Tedesco, M. and Fettweis, X.: Unprecedented atmospheric conditions (1948–2019) drive the 2019 exceptional melting season over the Greenland ice sheet, The Cryosphere, 14, 1209–1223, https://doi.org/10.5194/tc-14-1209-2020, 2020.

Tedesco, M., Fettweis, X., van den Broeke, M. R., van de Wal, R. S. W., Smeets, C. J. P. P., van de Berg, W. J., Serreze, M. C., and Box, J. E.: The role of albedo and accumulation in the 2010 melting record in Greenland, Environmental Research Letters, 6, 014 005, https://doi.org/10.1088/1748-9326/6/1/014005, 2011.

Tedesco, M., Fettweis, X., Mote, T., Wahr, J., Alexander, P., Box, J. E., and Wouters, B.: Evidence and analysis of 2012 Greenland records from spaceborne observations, a regional climate model and reanalysis data, The Cryosphere, 7, 615–630, https://doi.org/10.5194/tc-7-615-2013, 2013.

Tedesco, M., Mote, T., Fettweis, X., Hanna, E., Jeyaratnam, J., Booth, J. F., Datta, R., and Briggs, K.: Arctic cut-off high drives the poleward shift of a new Greenland melting record, Nature Communications, 7, https://doi.org/10.1038/ncomms11723, 2016.

van den Broeke, M. R., Enderlin, E. M., Howat, I. M., Munneke, P. K., Noël, B. P. Y., van de Berg, W. J., van Meijgaard, E., and Wouters, B.: On the recent contribution of the Greenland ice sheet to sea level change, The Cryosphere, 10, 1933–1946, https://doi.org/10.5194/tc-10-1933-2016, 2016.

van den Broeke, M. R., Kuipers Munneke, P., Noël, B., Reijmer, C., Smeets, P., van de Berg, W. J., and van Wessem, J. M.: Contrasting current and future surface melt rates on the ice sheets of Greenland and Antarctica: Lessons from in situ observations and climate models, PLOS Climate, 2, e0000 203, https://doi.org/10.1371/journal.pclm.0000203, 2023.

Vandecrux, B., MacFerrin, M., Machguth, H., Colgan, W. T., van As, D., Heilig, A., Stevens, C. M., Charalampidis, C., Fausto, R. S., Morris, E. M., Mosley-Thompson, E., Koenig, L., Montgomery, L. N., Miège, C., Simonsen, S. B., Ingeman-Nielsen, T., and Box, J. E.: Firn data compilation reveals widespread decrease of firn air content in western Greenland, The Cryosphere, 13, 845–859, https://doi.org/10.5194/tc-13-845-2019, 2019.

Vizcaíno, M., Mikolajewicz, U., Jungclaus, J., and Schurgers, G.: Climate modification by future ice sheet changes and consequences for ice sheet mass balance, Climate Dynamics, 34, 301–324, https://doi.org/10.1007/s00382-009-0591-y, 2009.

Wingham, D., Rapley, C., and D, G.: New Techniques in Satellite Altimeter Tracking Systems, in: Digest - International Geoscience and Remote Sensing Symposium (IGARSS), vol. ESA SP-254, pp. 1339–1344, Zurich, 1986.

https://doi.org/10.5194/egusphere-2024-3251
Preprint. Discussion started: 13 November 2024

615 Zwally, H. J., Abdalati, W., Herring, T., Larson, K., Saba, J., and Steffen, K.: Surface Melt-Induced Acceleration of Greenland Ice-Sheet Flow, Science, 297, 218–222, https://doi.org/10.1126/science.1072708, 2002.